Available online at www.sciencedirect.com
ScienceDirect
Geochimica et Cosmochimica Acta 70 (2006) 6079–6102
Geochimica
www.elsevier.com/locate/gca

Testing the relation between UV–vis color and TiO_2 content of the lunar maria

Jeffrey J. Gillis-Davis *, Paul G. Lucey, B. Ray Hawke

University of Hawai'i at Manoa, Hawai'i Institute of Geophysics and Planetology, 1680 East-West Road, Post 504, Honolulu, HI 96822, USA

Received 1 November 2005; accepted in revised form 28 August 2006

Abstract

Reflectance spectroscopy is important for placing lunar samples into a regional and global geologic context. To this end, the ultraviolet–visible (UV–vis) color ratio, used to estimate the TiO_2 composition of mature mare basalts, has been one of the most widely used spectral parameters in lunar exploration. We examine the correlation between UV–vis color and TiO_2 content using a combination of Clementine, Lunar Prospector, and sample data to document the extent to which color is dependent upon TiO_2. Examination of the remotely sensed data reveals that the correlation between UV–vis ratio and TiO_2 composition is best represented by a sigmoidal trend rather than the canonical linear or curvilinear correlation. With this information, we are then able to evaluate between two models that propose different explanations for the relationship between UV–vis color and TiO_2. The first model attributes the correlation between TiO_2 and UV–vis color to spectrally neutral opaques (i.e., ilmenite), while the other emphasizes the effect of Fe–Ti charge-transfer in lunar glasses and dual scattering mechanisms between high- and low-Ti basalts. We do not find evidence in the spectral data to support the occurrence of Fe–Ti charge-transfer in lunar glass as the principal cause for color in high-Ti basalts. The data also do not substantiate the existence of different scattering mechanisms (e.g., volume v. surface scattering) between high- and low-TiO_2 basalts. Instead, our analyses substantiate that the spectral effects of ilmenite exhibit a major influence over the UV–vis ratio. By including sample data we find that in addition to ilemenite/TiO_2 content, factors such as FeO content, ilmenite grain size, modal abundance of plagioclase, and the olivine-to-pyroxene ratio in a mare soils can influence the UV–vis continuum. These findings point to promising avenues of research that future UV–vis spectral techniques can exploit in order to yield more accurate TiO_2 estimates and potentially additional petrologic information.

1. Introduction

Multispectral imaging of the lunar maria reveals strong variations in the ratio of ultraviolet (400–560 nm) to visible (560–950 nm) wavelengths—the exact values of the ultraviolet–visible (UV–vis) ratio varies depending upon the particular citation (e.g., 402/564 nm (Charette et al., 1974); 380/560 nm (Pieters et al., 1976); 400/730 nm (Melendrez et al., 1994); and, as used herein, 450/750 using Clementine data (Blewett et al., 1997)). These multiple color units are undoubtedly lava flows of different composition (Whitaker, 1972; McCord et al., 1976; Pieters et al., 1980). Robert Strom suggested that the strong UV–vis variations are due to the major compositional variable in mare basalts, the Ti content (Whitaker, 1972). Charette et al. (1974) first showed that Ti content is correlated with telescopic measurements of UV–vis ratio in mature (agglutinate-rich) basaltic regolith, whereby samples with high-TiO_2 concentrations (e.g., derived from Mare Tranquillitatis) exhibit relatively flatter and "bluer" UV–vis slopes than basalts with lower concentrations in TiO_2 (e.g., central Mare Serenitatis), which are spectrally redder. The Charette Relation, or variations thereof, have been widely used to produce maps of the TiO_2 composition of mature mare basalts from multispectral imagery (e.g., Johnson et al., 1977; Pieters,

* Corresponding author.
E-mail address: gillis@higp.hawaii.edu (J.J. Gillis-Davis).

0016-7037/$ - see front matter © 2006 Elsevier Inc. All rights reserved.
doi:10.1016/j.gca.2006.08.035

1978; Johnson et al., 1991b; Melendrez et al., 1994; Lucey et al., 1998; Gillis et al., 2003).

However, uncertainties in the Charette Relation were revealed with failure to accurately predict the low-Ti contents of the Luna 24 basalts. Using Earth-based remotely sensed spectral data, Pieters et al. (1976) suggested that Mare Crisium contained 3–4 wt.% TiO_2. However, analysis of samples returned from Mare Crisium by the unmanned Soviet Luna 24, showed that these soils contain ~1 wt.% TiO_2 (Blanchard et al., 1978; Papike and Vaniman, 1978). A general consensus emerged that the relationship between color and TiO_2 was uncertain at low-concentrations of titanium (Fig. 1). Subsequent revisions to the Charette Relation were made in an attempt to reduce uncertainties at low TiO_2 concentrations by improving spectral contrast (Johnson et al., 1977; Johnson et al., 1991b,a), and spatial resolution (0.28 km/pixel (Melendrez et al., 1994)), but the correlation between TiO_2 and UV–vis spectral properties still contained large uncertainties particularly at low-Ti concentrations (Pieters, 1993). As such, Mare Crisium remains an important exception to the relationship as its low-Ti surface exhibits intermediate UV–vis spectral slope.

The Charette Relation is not the only method for predicting TiO_2 concentration of lunar soils from spectral data however. New spectral algorithms have been developed to estimate the Ti content for both highlands and mare, as well as mature and immature surfaces (Blewett et al., 1997; Lucey et al., 1998; Lucey et al., 2000a; Gillis et al., 2003). However, Gillis et al. (2003) and Elphic et al. (2002) have shown that TiO_2 maps derived using these new algorithms exhibit systematic errors. A likely reason for this uncertainty is that the UV–vis–TiO_2 correlation remains a fundamental component of these new algorithms. Therefore, it is important to investigate factors that give rise to and detract from the relationship between UV–vis color and TiO_2.

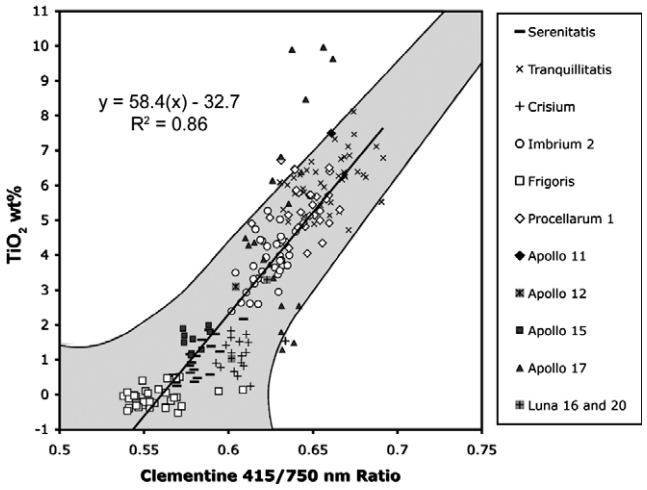

Fig. 1. Relation between Clementine UV–vis ratio and Lunar Prospector neutron spectrometer TiO_2 data, both at 15 km/pixel resolution, for selected regions of interest (ROI), the locations of which are shown in Fig. 2. Also plotted are average TiO_2 soil compositions for Apollo and Luna mare landing sites and sampling stations along with Clementine UV–vis ratio spectra (100 m resolution) from corresponding locations, data from Table 3 (Lucey et al., 2000a; Gillis et al., 2003). A best-fit linear regression to the ROI data is shown (straight black line). The gray area approximates the increasing uncertainty of predicting TiO_2 composition from remote UV–vis ratio measurements for mature mare regions as TiO_2 composition decreases, after Pieters (1993). On the basis of limited data sampling, a good linear or curvilinear correlation can be found to exist between UV–vis ratio and TiO_2 composition. To test the extent of this correlation we present UV–vis ratio and TiO_2 data for 18 ROIs, which total 3159 pixels at 15 km resolution.

Two qualitative models propose explanations for the relationship between UV–vis color and TiO_2, and are testable with data present herein (Section 4). First, the optical properties of spectrally neutral opaques are credited with causing the relationship between UV–vis spectral slope and TiO_2 (Wells and Hapke, 1977; Rava and Hapke, 1987). Ilmenite, the principal oxide phase, is dark and spectrally neutral relative to the spectrally red mature lunar mare soils. In this model, increasing amounts of ilmenite would decrease the spectral slope of mature mare soils, decrease the reflectance of an iron-bearing regolith, and reduce the spectral contrast. Therefore, adding ilmenite causes the comparatively red spectrum of low-Ti mature mare basalt soils to become flatter and appear bluer, resulting in a correlation with Ti-content. The lack of a perfect correlation between TiO_2 and UV–vis ratio suggests that factors controlling spectral variations are more complex than presumed by this model.

Pieters (1978) and more recently Pieters (1993) offered an explanation both for the general UV–vis–TiO_2 correlation, and its apparent breakdown at low-Ti contents. This second model emphasizes the effect of dark components, particularly Ti- and Fe-bearing glasses, finely dispersed Fe^0, and perhaps ilmenite present in the soils. In this view, Ti–Fe charge transfer bands darken the glass as Ti increases in lunar soils (Bell et al., 1976; Burns et al., 1976), thus creating a steep absorption edge from the visible to the ultraviolet and reducing the spectral contrast of the Ti-rich soils relative to Ti-poor mare soils. Also in this model, components of Ti-rich soils, particularly glass, ilmenite, and submicroscopic Fe^0, are so dark that surface scattering rather than volume scattering dominates reflectance. As a result, compositional variations other than Ti are imperceptible in high-Ti basaltic soils, as the actual spectral properties of the individual soil components are masked due to the high spectral scattering component. In brighter low-Ti soils, however, volume transmission occurs more commonly and the inherent spectral properties of the basalts become much stronger, allowing color variations caused by a variety of compositional factors to become dominant. Since different glass and mineral phases have different spectral properties in the visible, at low-TiO_2 concentrations, the true colors and associated complexity of soil mineralogy are observed causing the observed scatter in the correlation.

Since the conception of the Charette Relation and most of the subsequent work, a large amount of new data has become available. Progress in understanding of the

compositional nature of lunar soils continues at a steady pace and application of new tools has recently led to much better understanding of the compositional and optical properties (Taylor et al., 2001b; Pieters et al., 2002). Critical to this progress is the availability of Lunar Prospector and Clementine data, which allow direct inspection of the relationship between Ti and lunar color for all mare surfaces.

It is the purpose of this paper to present a reassessment of the relationship between color and Ti using Clementine and Lunar Prospector data. These data are used to quantitatively test previous models that attempt to explain the Charette Relationship as it was understood at the time, to systematically examine the efficacy of the components that may affect lunar color, and to suggest areas of future research that may lead to achieving Charette's original goal—to map the Ti content of the lunar mare with high fidelity.

Improving the accuracy and precision of TiO_2 estimates in mare soils will yield several benefits for lunar science. A first-order result is a better understanding of lateral and vertical compositional heterogeneity of the mantle with respect to TiO_2, which as consequence provides a more accurate estimate of the composition of the mantle, as its composition is inferred from mare basalts. Second, plans for in-situ resource utilization will profit by accurate resource assessment of ilmenite abundance, as ilmenite is efficient at retaining solar wind-implanted volatiles (Taylor, 1994), and can be utilized for oxygen production.

2. Data

The Clementine Mission (Nozette and The Clementine Team, 1994) acquired multispectral data (415, 750, 900, 950, 1000, 1100, 1250, 1500, 2000, 2600, and 2700 nm) at ~200 m/pixel resolution. For our analyses, we used the UV–vis (Lee, 1997; Eliason et al., 1999), and near infrared digital (http://astrogeology.usgs.gov/Projects/Clementine-NIR/) image models produced by the USGS, Flagstaff.

The Lunar Prospector spacecraft (Binder, 1998) obtained data that is used to estimate Fe and Ti concentrations using the gamma-ray (Lawrence et al., 2002; Prettyman et al., 2006) and neutron spectrometers (Elphic et al., 2002). Both TiO_2 data sets were acquired during the low altitude (30 ± 15 km) portion of the mission, however, the map resolution of the two data sets is different. The gamma-ray data are binned into $2° \times 2°$ (60×60 km) pixels, at the equator, while the neutron spectrometer data are parsed into $0.5° \times 0.5°$ (15×15 km) pixels. For our analyses, we chose to use the neutron derived TiO_2 data for comparisons with Clementine UV–vis ratio data because the neutron derived TiO_2 data exhibit a narrower range in TiO_2 values for a given mare area, better spatial resolution, and lower relative uncertainty than the gamma-ray data (5% versus 15% relative uncertainty). The data used in this study represent spectrometer-reduced data as of June 2002. We acknowledge that these data are an iterative product and that subsequent data releases by the Lunar Prospector Science Team may be more accurate (reduced versions of Lunar Prospector spectrometer data are available at the Planetary Data System archive http://pds-geosciences.wustl.edu/missions/lunarp/index.htm).

Although the Lunar Prospector neutron data are of low-spatial resolution relative to the Clementine data, the connection between the neutron signal and titanium is well understood, unlike the case for the spectral data, as we will discuss. In addition, the neutron data offer independent, global measurements of TiO_2 that serve as ground-truth comparisons to Clementine UV–vis data in this investigation. The Clementine spectral reflectance and Lunar Prospector data are coregistered and resampled to the resolution of the neutron spectrometer data, half-degree per pixel. Integrating these two data sets allows us to characterize the relation between TiO_2 content and Clementine spectral reflectance data. So whereas before there were only 6 ground-truth points in the Charette Relation (4 Apollo and 2 Luna missions to the maria), we employ over 33,200 data points (i.e., all areas with >11 wt.% FeO using Lunar Prospector neutron spectrometer data at half-degree resolution) to understand the correlation between UV–vis and TiO_2.

Improving the concordance between the Lunar Prospector and Clementine data sets for TiO_2 will provide a means to extend compositional information to the spatial resolution of the Clementine data (~200 m/pixel), which is almost 2 orders of magnitude better than Lunar Prospector. Soon even this resolution will be improved upon, as future missions will provide even higher resolution multispectral data (e.g., SMART-1, SELENE, Chandrayaan-1, Chang'e-1, and Lunar Reconnaissance Orbiter).

A basic premise of the Charette Relation is that it is only applicable to mature mare surfaces; to avoid highland contamination (both spectral and physical), we established 18 regions of interest (ROI) that are contained entirely within major mare exposures distant from highland contacts and confine our analysis to data from these regions. This approach allows minimization of compositional mixing effects due to vertical and lateral impact mixing, as well as scattered light effects in the Clementine data set. Impact mixing has an effect over short distances, with the most extensive mixing occurring within 2 km of the contact and less mixing occurring within 10 km of the contact (Rhodes, 1977; Mustard and Pieters, 1989). However, Apollo 11 soils exhibit non-trivial amounts of highlands contamination even at distances of 50 km from the mare-highlands boundary. Estimates for the proportion of non-mare material in the Apollo 11 <1-mm fines is approximately 23% (Korotev and Gillis, 2001), and the difference between sample measured and soil measured TiO_2 composition is 23.7% (Giguere et al., 2000). Twenty-percent is probably a good approximation of background contamination of the maria by highlands, with exception of Oceanus Procellarum where it is likely less because of its broad lateral extent. Mitigating highland contamination above the

background level is important as the highlands clearly obey a different relationship (their low-Ti surfaces exhibit UV–vis ratios that are intermediate to the mare surfaces).

On the other hand, scattered light affects data in high-contrast regions (e.g., mare-highland boundaries). Where light is scattered from outside the field-of-view of the charge-coupled device (CCD) but still inside the field-of-view of the optics. The result is an increase in the absolute radiance of the image (Robinson, 2001). The amount of scattered light varies as a function of wavelength, distance from the edge of a mare-highland boundary, and contrast of the lunar surface within the field of view of the imaging system. As a result, ratios of two wavelengths along high-contrast boundaries could introduce spectral artifacts. Scattered light would affect data taken from a distance of ~1 or less Clementine image width and/or height, or $\sim 77 \times 58$ km at 0.2 km/p resolution, from a mare-highland boundary. Using ROIs reduces the potential for highlands contamination and scattered light because most data are selected >60 km from a mare-highland boundary, with exception of Mare Frigoris and Lacus Somniorum.

The ROIs are distributed throughout all major nearside mare (Fig. 2), with some named maria being represented by several ROIs (e.g., Imbrium and Procellarum). Each ROI represents a major spatially contiguous area of uniform UV–vis color. Regions of interest were selected on the basis of uniform color in an effort to reduce maturity, contamination, and scattered light effects, and to separate mare localities into ROIs with a similar UV–vis color properties and therefore composition. These ROIs range in size from 22,000 to 90,500 km^2, with the average ~40,000 km^2. Together the ROIs represent a combined total of 3159 half-degree mare points, and their average characteristics are summarized in Tables 1 and 2. Collectively, these ROIs represent an array of locations with varying properties (e.g., mineralogy and chemistry gained from sample and remotely sensed data) that can be systematically evaluated in order to investigate their effects on UV–vis color.

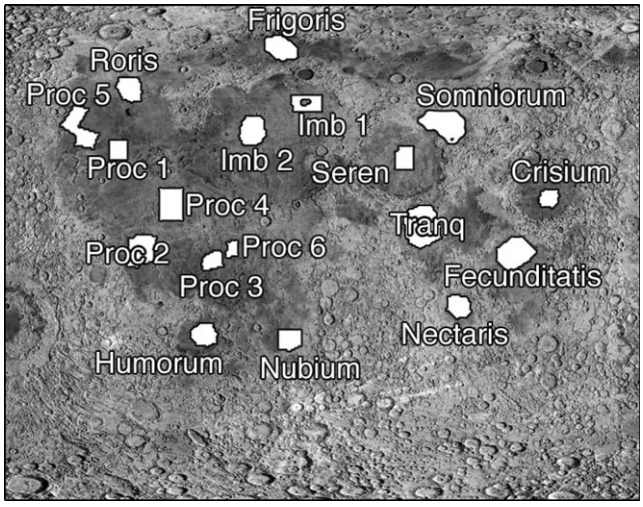

Fig. 2. Nearside shaded relief map of the Moon (90 °W–90 °E; 70 °S–70 °N) showing locations and area that data for each of the 18 ROIs were collected. Ancillary data for the regions of interest can be found in Tables 1 and 2.

3. Results

3.1. A new relationship between TiO_2 and UV–vis ratio

The data from the 18 individual regions of interest reveal a previously unrecognized sigmoidal relationship between TiO_2 and UV–vis color (Fig. 3). The sigmoidal relation can be divided into three trends, illustrated in the Fig. 4, however, we cannot confidently determine whether the shallowing of the steep black-lined trend, as a result of the Tranquillitatis data, is truly a third trend—more confidence would be placed in the Tranquillitatis trend if the neutron TiO_2 data were at high enough resolution to plot the Apollo 17 site in Figs. 3 and 4 to observe whether it plots with the Apollo 11 data or with the Apollo 17 sample data. Our hesitation in designating the upper trend as separate trend is in response to the fact that full-resolution Clementine data of Apollo 17 site plot as a continuation of the middle TiO_2 trend. On this basis, we suggest that the UV–vis–TiO_2 relation is best characterized by two trends: a shallow trend that corresponds to low-Ti basalts (gray line in Fig. 4), and a steeper slope that represents moderate- and high-Ti basalts (black line in Fig. 4). A transition between the two slopes occurs at approximately 1 wt.% TiO_2 and at UV–vis ratio of 0.61. This inflection is close to the UV–vis ratio criteria established by Gillis et al. (2003) for determining which of two empirical equations would be used to calculate TiO_2 composition from Clementine data. Where a logic test was applied that stated, if the 415/750 ratio is >0.59 and the 415 nm reflectance is <0.065, then use an alternate algorithm to Lucey et al. (2000a). This alternate TiO_2 algorithm was developed by Gillis et al. (2003) to yield more accurate TiO_2 estimates for darker, bluer soils (e.g., Apollo 11, and Luna 20 and 24) than Apollo 17 mare soils (Table 1).

The sigmoidal relation is notably different than the single curvilinear trend of Charette et al. (1974) or subsequent revisions (Johnson et al., 1977; Johnson et al., 1991a,b; Pieters, 1993; Melendrez et al., 1994), but reminiscent of the shaded relationship of Pieters (1993) indicating higher uncertainty at low-Ti (e.g., Fig. 1). As the above workers have noted, there are larger variations in color for low-titanium values than for high-titanium soils. Where TiO_2 compositions <2 wt.% can vary by ~10% in UV–vis ratio values, while UV–vis ratios of high-Ti basalts (e.g., Apollo 11 and 17) vary by ~5%. In contrast to previous observations with sparser data, we find that color values for high-Ti soils (>5 wt.%) are also quite variable. Interestingly, the lowest scatter in color is at intermediate Ti values (2–4 wt.%).

A focus on predictability yields new insights regarding the utility of the spectral data. Previous discussions have emphasized the color variations at particular Ti contents.

Table 1
Ancillary and compositional data for the 18 regions of interest (ROI) in Figs. 2–4

Mare ROI	# pixels	Area (km^2)	Center Lat.[a]	Center Lon.[a]	FeO wt.%	TiO_2wt.%	FeO + TiO_2 wt.%	415/750 nm	Trend[b]	Logical[c]
Somniorum	113	25,425	37.0	32.0	12.0 ± 0.7	1.1 ± 0.2	13.1	0.5668 ± 0.010	Lower	False
Nectaris	143	32,175	−16.0	36.0	13.5 ± 0.9	1.0 ± 0.4	14.5	0.6088 ± 0.008	Lower	False
Frigoris	200	45,000	57.0	−11.0	15.2 ± 0.5	−0.1 ± 0.3	15.1	0.5569 ± 0.014	Lower	False
Sinus Roris	175	39,375	46.0	−61.0	16.4 ± 0.7	0.6 ± 0.4	16.9	0.5485 ± 0.010	Lower	False
Procellarum 5	230	51,750	33.0	−70.0	15.9 ± 1.4	1.1 ± 0.5	17.1	0.5831 ± 0.009	Lower	False
Serenitatis central	134	30,150	27.0	20.0	17.5 ± 0.7	0.6 ± 0.3	18.1	0.5758 ± 0.007	Lower	False
Imbrium 1	149	33,525	41.0	−7.0	17.5 ± 1.5	0.6 ± 0.5	18.1	0.5469 ± 0.006	Lower	False
Crisium	98	22,050	15.0	59.0	17.5 ± 0.9	0.7 ± 0.2	18.2	0.6067 ± 0.018	Lower	True
Nubium	121	27,225	−25.0	−13.0	16.6 ± 0.9	2.2 ± 0.4	18.8	0.6205 ± 0.009	Upper	False
Fecunditatis	294	66,150	−5.0	50.0	17.0 ± 0.9	1.9 ± 0.3	18.9	0.6173 ± 0.009	Upper	True
Procellarum 6	54	12,150	6.0	−150.0	17.1 ± 1.6	2.7 ± 0.6	19.8	0.6130 ± 0.007	Upper	False
Humorium	159	35,775	−25.0	−37.0	18.2 ± 1.5	2.5 ± 0.3	20.7	0.6227 ± 0.011	Upper	True
Tranquillitatis	402	90,450	8.0	27.0	17.3 ± 0.9	6.1 ± 1.1	23.4	0.6634 ± 0.017	Upper	True
Procellarum 2	244	54,900	1.0	−52.0	21.2 ± 1.7	2.5 ± 0.6	23.7	0.6232 ± 0.007	Upper	True
Procellarum 3	95	21,375	0.0	−40.0	20.1 ± 1.8	3.9 ± 0.6	24.9	0.6315 ± 0.006	Upper	True
Imbrium 2	202	45,450	34.0	−21.0	21.3 ± 0.8	4.4 ± 0.5	25.6	0.6259 ± 0.008	Upper	True
Procellarum 4	247	55,575	12.0	−46.0	21.7 ± 1.3	5.6 ± 0.5	27.2	0.6363 ± 0.010	Upper	True
Procellarum 1	99	22,275	24.0	−59.0	22.2 ± 1.2	5.2 ± 0.5	27.4	0.6470 ± 0.017	Upper	True

FeO and TiO_2 data are from the Lunar Prospector Neutron Spectrometer (Elphic et al., 2002).
[a] Negative latitude is west and negative longitude is south.
[b] Trend refers to the upper and lower trend as defined by the data from the 18 ROIs in Fig. 4.
[c] Logical statement used by Gillis et al. (2003) to determine which of two trends to use in calculating TiO_2 wt.% (True ≡ Apollo 11 trend was used).

Table 2
Average Clementine reflectance values for the 18 ROIs in Figs. 2–4

Mare ROI	415 nm	750 nm	900 nm	950 nm	1000 nm	1100 nm	1250 nm	1500 nm	2000 nm	2200 nm	2700 nm
Somniorum	0.0830	0.1462	0.1509	0.1533	0.1587	0.1714	0.1932	0.2174	0.2562	0.3440	0.9931
Nectaris	0.0787	0.1293	0.1335	0.1335	0.1385	0.1489	0.1658	0.1821	0.2118	0.2922	0.8978
Frigoris	0.0837	0.1502	0.1488	0.1479	0.1527	0.1707	0.1954	0.2227	0.2629	0.4026	1.0340
Sinus Roris	0.0716	0.1306	0.1326	0.1329	0.1370	0.1491	0.1715	0.1957	0.2385	0.3560	0.9886
Procellarum 5	0.0654	0.1121	0.1148	0.1157	0.1197	0.1280	0.1439	0.1607	0.1996	0.3028	0.8915
Serenitatis Central	0.0624	0.1083	0.1097	0.1105	0.1145	0.1206	0.1409	0.1600	0.1875	0.2752	0.8535
Imbrium 1	0.0660	0.1207	0.1217	0.1218	0.1262	0.1379	0.1577	0.1823	0.2207	0.3404	0.9687
Crisium	0.0617	0.1018	0.1049	0.1059	0.1089	0.1159	0.1306	0.1439	0.1711	0.3181	0.8164
Nubium	0.0662	0.1067	0.1090	0.1093	0.1129	0.1191	0.1323	0.1459	0.1752	0.2629	0.8555
Fecunditatis	0.0621	0.1006	0.1038	0.1044	0.1068	0.1141	0.1273	0.1343	0.1607	0.2541	0.7308
Humorium	0.0597	0.0959	0.0965	0.0965	0.0992	0.1062	0.1194	0.1304	0.1497	0.2196	0.7952
Procellarum 3	0.0705	0.1129	0.1148	0.1141	0.1164	0.1245	0.1346	0.1461	0.1688	0.2470	0.7586
Tranquillitatis	0.0588	0.0887	0.0920	0.0930	0.0954	0.0998	0.1092	0.1141	0.1427	0.2110	0.7258
Procellarum 2	0.0558	0.0896	0.0916	0.0913	0.0932	0.0999	0.1095	0.1201	0.1428	0.2314	0.7185
Imbrium 2	0.0603	0.0964	0.0974	0.0968	0.0987	0.1059	0.1190	0.1323	0.1597	0.2533	0.7974
Procellarum 4	0.0609	0.0957	0.0964	0.0953	0.0966	0.1027	0.1136	0.1240	0.1435	0.2389	0.7632
Procellarum 1	0.0611	0.0946	0.0961	0.0957	0.0974	0.0970	0.1089	0.1203	0.1498	0.2317	0.7560

However, the utility of the multispectral data is in the prediction of Ti from color, rather than the spectroscopically interesting color effects at a given Ti content. At the lowest color values, (UV–vis ratio <0.58) all Ti values are <2 wt.% (Figs. 3 and 4), so very low color values do indicate low Ti, however, all low Ti surfaces do not have low color values. For instance, UV–vis ratios as high as 0.64 exist for some low-Ti basalts, <2 wt.% TiO_2. Similarly, at high color values (UV–vis ratio >0.66) all Ti values are uniformly high, >5 wt.%, but again high-Ti surfaces exist with lower color values. At intermediate UV–vis ratios, Ti varies across nearly its entire range of values (Figs. 3 and 4).

The uncertainty in prediction of Ti content can be mapped (Fig. 5). High confidence is assigned to UV–vis ratio values <0.58 or >0.66. Regions with a high confidence level are mapped as gray (low-Ti) or black (high-Ti). The highest TiO_2 uncertainties are observed for mare soils with intermediate UV–vis values, between 0.58 and 0.66, which are mapped in the herringbone pattern. In this UV–vis ratio range, TiO_2 can vary unpredictably from 0 to 7.4 wt.%, with a mean of 2.2 and a standard deviation of ±1.6. On this basis, we suggest that UV–vis color can place a lower limit on the distribution of high- and low-Ti basalts, but it may not capture all basalts of these compositions. Fur-

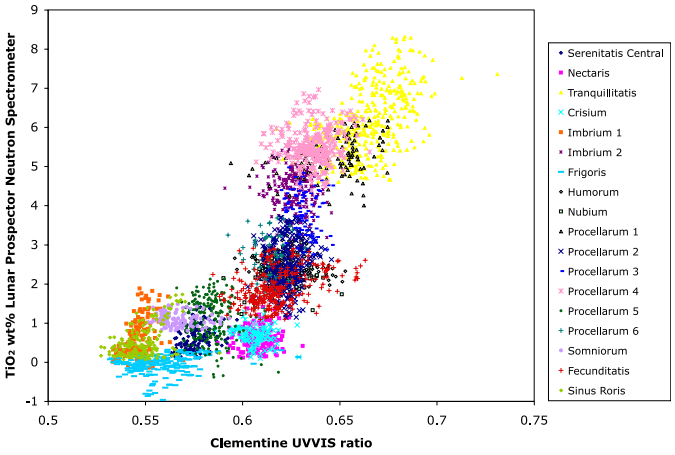

Fig. 3. Lunar Prospector neutron spectrometer TiO_2 and Clementine UV–vis ratio data for the 18 ROIs shown in Fig. 2. These data reveal an apparent non-linear, sigmoidal shape to the UV–vis–TiO_2 correlation. Regions of interest were selected on the basis of uniform color, in an effort to reduce error as a result of physical and spectral mixing. Ancillary data for the regions of interest can be found in Tables 1 and 2.

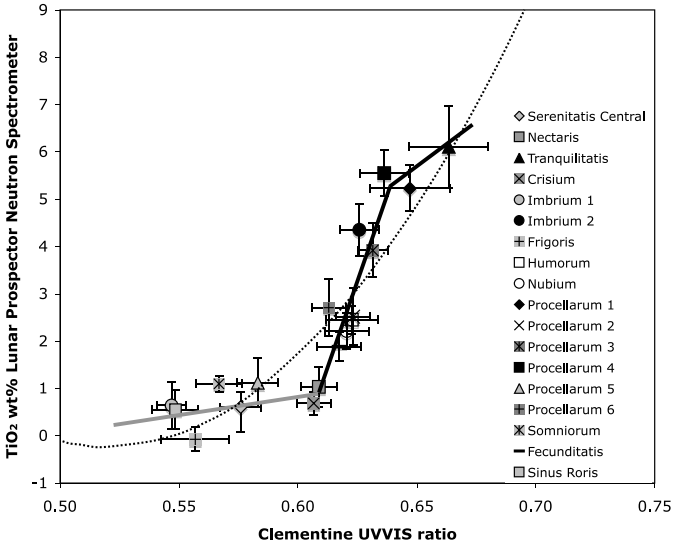

Fig. 4. Average TiO_2 compositions (Lunar Prospector neutron spectrometer) and UV–vis ratio data (Clementine) and one-sigma standard deviation reported for the 18 ROIs shown in Figs. 2 and 3. The dotted curve represents an approximated Charette Relation trend, gray line represents the low-Ti trend, and the black kinked line denotes the moderate- and high-Ti trend.

thermore, nothing confident can be said about the basalts that have intermediate color values, which cover the vast majority of the maria (75%). This large area of uncertainty is in agreement with the finding of Gillis et al. (2003) that showed TiO_2 compositions for over two-thirds of maria were over or underestimated by algorithms of Lucey et al. (2000a). This result would affect the absolute position of the unimodal TiO_2 histogram plot presented by Giguere et al. (2000) and Gillis et al. (2003). Which is to say that the absolute TiO_2 mode and/or the width of the mode may change, not that a bimodal distribution will be created from the unimodal distribution, as the Lunar Prospector neutron and gamma-ray

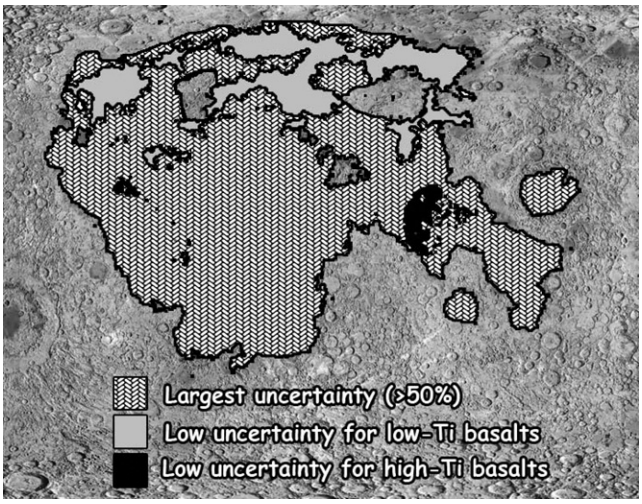

Fig. 5. Nearside shaded relief map (90 °W–90 °E; 70 °S–70 °N) showing the relative uncertainty in estimated TiO_2 for mare basalts as determined using the UV–vis ratio (Figs. 3 and 4). From this illustration, we find that the prediction of TiO_2 from color is highly uncertain for ~75% of mare surfaces (herringbone pattern).

spectrometer data (Elphic et al., 2002; Prettyman et al., 2006) do not exhibit a bimodal distribution.

3.2. The origin of the sigmoid pattern

The observed sigmoid structure in Figs. 3 and 4 begs explanation. This pattern could arise from the interaction of several subtrends, but we favor the notion that the pattern is composed of two, partly overlapping trends, a lower trend and an upper trend. Again, we include the tail of the sigmoid as part of the upper trend because the data do not substantiate whether it is its own trend. Basalts within the lower trend contain lower TiO_2 (<1.5 wt.%) and FeO contents (12.0–17.5 wt.%) than basalts of the upper slope (>1.5 wt.% TiO_2; 16.6–22.2 wt.% FeO). The two spectral trends are also divided on the basis of the sum of FeO + TiO_2 (Table 1). Mare areas the lie along the upper trend exhibit FeO + TiO_2 values $\geqslant$18.5 wt.%, while the sum of FeO + TiO_2 for mare areas along the lower trend $\leqslant$18.5 wt.%. Although the sum of FeO and TiO_2 is not necessary to distinguish between the two trends, as Figs. 3 and 4 show, assessing both FeO and TiO_2 allows variations due to FeO within a single trend (upper or lower) to also be discriminated (e.g., FeO differences between Apollo 15 and Luna 24 basalts). The FeO + TiO_2 discrimination may relate to the bulk composition of the parent magma and the crystallization sequence the melt undergoes. The interval over which Fe–Ti oxide occur in the crystallization sequence is dependent upon the FeO and TiO_2 content of the melt (Papike and Vaniman, 1978). For example, for the Apollo 17 high Mg# samples (e.g., 74275, Mg# = 0.5) the apparent crystallization sequence was olivine + spinel $\Rightarrow$ armalcolite + pyroxene + ilmenite + plagioclase, however, for more iron-rich samples (e.g., 70215, Mg# = 0.43) crystallization of the Fe–Ti oxides overlapped

with part of the olivine crystallization interval (armalcolite + ilmenite ⇒ olivine + spinel ⇒ plagioclase). Pyroxenes from both samples have similar SiO_2, Al_2O_3, and TiO_2 composition but sample 70215 has 2 wt.% more FeO (8.1% v 10.2% (Dymek et al., 1975)). Fe and Ti contents affect the visible reflectance of silicate minerals; thus, pyroxenes and olivines become darker the more ferroan or titanian they become.

The steepness of the UV–vis ratio-TiO_2 composition slope is a distinguishing characteristic between the two trends; where variations in slope are a factor of the range of values for TiO_2 content and UV–vis ratio. For instance, basalts of the upper or high-Ti slope exhibit a steeper slope than the low-Ti basalts because they range from 1.5 to 8 wt.% TiO_2 over the same UV–vis ratio range as the lower slope (where the range in UV–vis ratio values is 0.075), which ranges from 0 to 1.5 wt.% TiO_2. Thus, basalts with >1.5 wt.% TiO_2 exhibit a steeper slope than the trend defined by the data for basalts with <1.5 wt.% TiO_2. Moreover, the position of the high-TiO_2 trend appears shifted to the left or appears redder than predicted on the basis of the slope of the low-TiO_2 trend (i.e., by inferring that the UV–vis ratio values for basalts of the lower trend would extend linearly to higher UV–vis ratio values if they were to contain >1.5 wt.% TiO_2).

Sample data supports the concept of a sigmoidal relation between TiO_2 composition and UV–vis ratio. The similarity between sample and remote sensing data is illustrated by comparing full-resolution Clementine UV–vis ratio spectra of Apollo 11, 12, 15, and 17, and Luna 16 and 24 landing sites and sampling stations with TiO_2 compositions from typical soils from these sites (Table 3). The combined sample-remote sensing data lie along the same sigmoidal trend defined by the ROI data (Fig. 6). This comparison reveals a first-order correlation between volume percent ilmenite and UV–vis ratio for soils that comprise the steeper trend (>0.61 UV/vis). UV–vis ratio values increase with increasing modal percentages of opaques; Apollo 12 olivine basalts and Luna 16 basalts contain 7.1% opaques, Apollo 12 ilmenite basalts (opaques = 9.1%); Apollo 17 low-K basalts (opaques = 15.1%), Apollo 11 high-K basalts (opaques = 20.6%) and very high-Ti basalts (opaques = 24.4%), where modal abundance is normalized to 100% for the four major mineral phases (e.g., olivine, pyroxene, plagioclase, and ilmenite). Apollo 17 high-Ti basalts are a notable exception. As noted previously (Gillis et al., 2003), the Apollo 17 soils exhibit higher reflectance values and similar UV–vis ratios relative Apollo 11 soils, which have similar to lower TiO_2 compositions (i.e., Apollo 17 soils should be bluer than Apollo

Table 3
Clementine reflectance and chemical compositions for the <1 mm soil fraction, and values of I_s/FeO[a] are an average of values from Morris (1978) for surface soils from corresponding Apollo and Luna landing sites and sample stations

Station	415 nm	750 nm	900 nm	950 nm	1000 nm	415/750	950/750	FeO meas.	TiO_2 meas.	I_s/FeO[a]
A11	0.0607	0.0918	0.0957	0.0971	0.0996	0.6609	1.057	15.8	7.5	74
A12	0.0701	0.1161	0.1182	0.1189	0.1231	0.6041	1.024	15.4	3.1	45
A15-LM	0.0726	0.1267	0.1306	0.1333	0.1380	0.5729	1.052	15.0	1.9	70
A15-S1	0.0760	0.1314	0.1333	0.1359	0.1400	0.5787	1.035	16.8	1.6	60
A15-S2	0.0863	0.1479	0.1519	0.1560	0.1604	0.5838	1.055	11.5	1.3	68
A15-S4	0.0741	0.1282	0.1314	0.1321	0.1378	0.5779	1.030	16.6	1.2	34
A15-S6	0.0800	0.1395	0.1443	0.1484	0.1528	0.5736	1.064	12.1	1.5	67
A15-S7	0.0780	0.1350	0.1406	0.1446	0.1492	0.5776	1.071	13.9	1.1	43
A15-S8	0.0719	0.1253	0.1292	0.1317	0.1367	0.5737	1.050	15.2	1.7	77
A15-S9	0.0740	0.1256	0.1240	0.1236	0.1270	0.5888	0.984	16.9	1.8	51
A15-S9a	0.0769	0.1307	0.1223	0.1211	0.1247	0.5880	0.926	20.4	2.0	28
A17-LM	0.0698	0.1082	0.1128	0.1142	0.1177	0.6457	1.056	16.6	8.5	51
A17-S1	0.0707	0.1068	0.1089	0.1097	0.1127	0.6617	1.027	17.8	9.6	34
A17-S5	0.0677	0.1061	0.1089	0.1115	0.1149	0.6375	1.050	17.7	9.9	37
A17-S7	0.0861	0.1387	0.1450	0.1476	0.1535	0.6206	1.064	11.6	3.9	80
A17-S8	0.0781	0.1277	0.1319	0.1363	0.1411	0.6116	1.068	12.3	4.3	80
A17-S9	0.0712	0.1108	0.1148	0.1163	0.1208	0.6429	1.050	15.4	6.4	71
A17-LRV1	0.0657	0.1039	0.1080	0.1094	0.1137	0.6325	1.053	16.3	8.0	60
A17-LRV2	0.0707	0.1149	0.1214	0.1229	0.1278	0.6151	1.069	13.4	4.4	81
A17-LRV3	0.0704	0.1108	0.1159	0.1192	0.1237	0.6355	1.076	14.8	5.5	85
A17-LRV7	0.0677	0.1072	0.1123	0.1146	0.1196	0.6310	1.069	16.1	6.8	54
A17-LRV8	0.0650	0.1042	0.1083	0.1109	0.1148	0.6243	1.065	15.7	6.6	67
A17-LRV9	0.0674	0.1076	0.1120	0.1153	0.1189	0.6260	1.071	14.6	6.1	71
A17-LRV10	0.0878	0.1407	0.1462	0.1503	0.1556	0.6242	1.068	11.2	3.7	70
A17-LRV11	0.0749	0.1229	0.1269	0.1303	0.1345	0.6098	1.060	12.7	4.5	68
A17-LRV12	0.0703	0.1071	0.1100	0.1104	0.1150	0.6562	1.031	17.4	10.0	41
L16	0.0624	0.1002	0.1046	0.1063	0.1092	0.6226	1.062	16.8	3.3	—
L24	0.0623	0.1035	0.1069	0.1077	0.1114	0.6016	1.041	19.6	1.0	—

References for laboratory analysis of soil samples listed in Table 4 of Jolliff (1999). Clementine spectra from (Blewett et al., 1997). Abbreviations: LM, Lunar Module; S, Station; LRV, Lunar Rover Stop; L, Luna.

[a] I_s/FeO is the Ferro magnetic resonance surface exposure index as defined by Morris (1978).

11). Multiple working hypotheses for the origin of the spectral differences between the Apollo 11 and 17 high-Ti basalts have been proposed (Gillis et al., 2003), but further investigation and testing are necessary in order to substantiate a single hypothesis. The correlation between ilmenite content and UV–vis ratio for the Apollo and Luna samples suggests that the UV–vis ratio of the upper slope, which the sample data encompass, is primarily the result of variations due to ilmenite. However, not all UV–vis variations correlate with TiO_2.

Plotting data for all mare basalts does produce a single trend with a low degree of correlation (Fig. 7). However, we suggest that such a trend is partially an artifact of mixing between geologic materials that comprise the two spectral trends. The "Mixing Zone" data in Fig. 8 represent contiguous areas along the boundary between high-Ti and high-FeO and low-Ti maria in the Imbrium-Procellarum region, and the border of Mare Serenitatis. Thus, mixing occurs between high-Ti, high-UV–vis ratio basalts (e.g., Procellarum 1 and Tranquillitatis) and low-Ti, low UV–vis ratio basalts (e.g., Frigoris and Imbrium 1) as opposed to mixing with low-Ti basalt of intermediate color (e.g., Mare Crisium or Fecunditatis). Without the mixing zone basalts, or with using the ROI data, the relation appears to be better characterized by two trends with basalts of intermediate color connecting them.

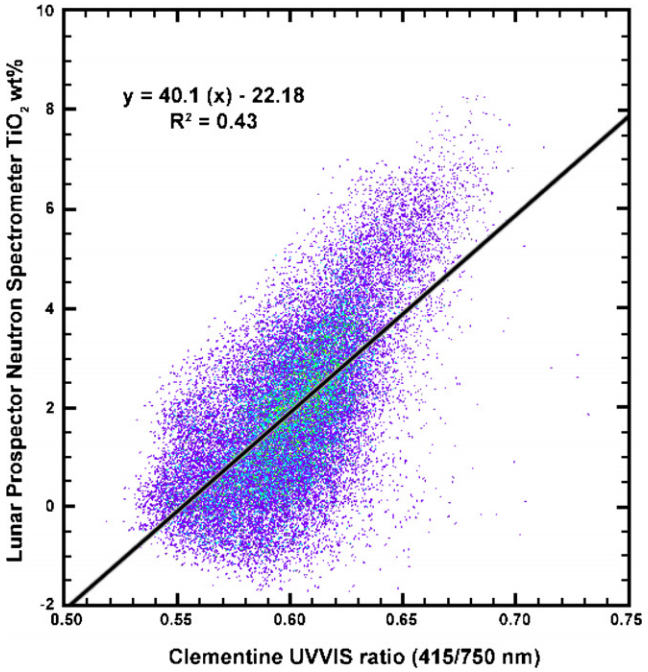

Fig. 7. Lunar Prospector neutron spectrometer data for TiO_2 plotted against the Clementine 415/750 nm ratio. Pixels plotted are $0.5° \times 0.5°$ at the equator and represent all mare areas with >11 wt.% FeO in the Lunar Prospector neutron spectrometer data (>32,000 data points). The black line represents a best-fit linear regression to all the data.

3.3. Do differences in data set uncertainty yield the UV–vis–TiO_2 trend?

The Clementine and Lunar Prospector data exhibit different uncertainties, 5% for the neutron TiO_2 data (Elphic et al., 2000) and ~1% for Clementine UV–vis data (McEwen and Robinson, 1997). Therefore the possibility of instrumental noise introducing scatter in the UV–vis–TiO_2 relationship (Fig. 7) was investigated (Gillis and Lucey, 2004). The contribution of systematic noise to the cor-

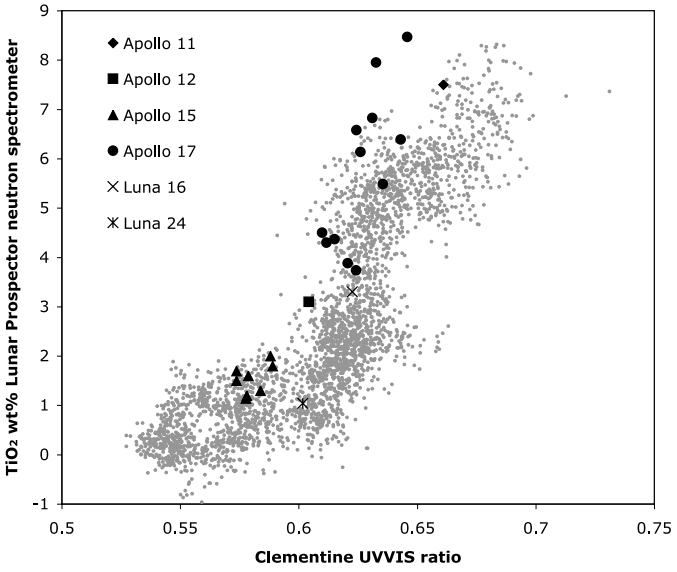

Fig. 6. Laboratory TiO_2 analysis for representative soils from Apollo and Luna landing sites and sampling stations compared with Clementine UV–vis 100 m/pixel data from corresponding locations (Table 3). The sample data exhibit a good correlation with compositional and spectral data from the 18 regions of interest (gray points).

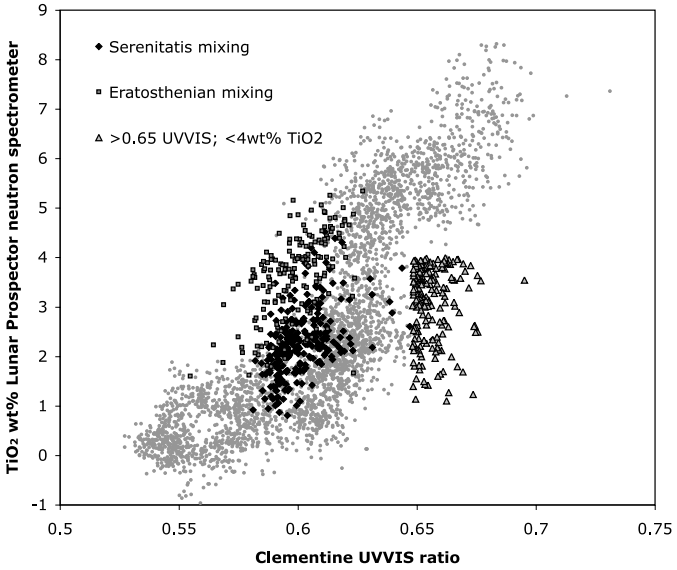

Fig. 8. Compositional and spectral data for "mixing zone basalts" and the 18 regions of interest (light-gray points). Adding the mixing zone basalts produces a trend more similar to Fig. 7. The mixing zone basalts occur along the border between the high-Ti and low-Ti basalts in Procellarum and Imbrium, eastern central mare Imbrium, the border of mare Serenitatis, and mare Cognitum.

relation was evaluated by comparing a synthetic Clementine UV–vis ratio data set with a calculated noise component added to the true Clementine UV–vis ratio data set that is presumed noiseless. It was found that the amount of simulated noise required to match the degree of correlation ($R^2 = 0.43$; Fig. 7) between TiO_2 and UV–vis ratio for all mare areas with >12 wt.% FeO was 5 to 6 times the reported uncertainty difference between the two instruments. Therefore, the scatter observed between the two data sets is not the result of differences in the precision of the two instruments.

4. New data, old hypotheses

The new data alter the landscape in which the previous models were formed; yet these models offer insights that are still highly relevant. In the view of Hapke and Rava, UV–vis variations result from spectrally neutral ilmenite altering the spectral properties of the basaltic regolith. With modern tools, mainly the result of Hapke's work, this hypothesis can be explored and weighed against the new data. The Pieters contrast reduction model can also be assessed in light of the new observations. Recent insights into the physical properties of lunar soils (e.g., Taylor et al., 1996; Keller and McKay, 1997) will also serve as data to test these theoretical models.

4.1. Examining whether ilmenite alone can account for the UV–vis–TiO_2 correlation

The suggestion by Rava and Hapke (1987) that ilmenite controls the UV–vis ratio is testable using radiative transfer modeling, by computing mixtures of ilmenite and ilmenite-free lunar soil and examining the relationship between Ti (carried by ilmenite) and color. For the ilmenite end-member we use a spectrum of ilmenite from the USGS spectral library (http://speclab.cr.usgs.gov/spectral.lib04/spectral-lib.desc+plots.html). The spectral properties of the low-Ti soil are represented by the mean of the Sinus Roris and Lacus Somniorum data points (Fig. 4), which show a near zero mean TiO_2 content, and are near the low-Ti, low-color value boundary of the data. Thus, the modeling spectrally mixes mature mare soil and plain ilmenite. We did not take into account possible effects of maturation on ilmenite grains (e.g., vapor deposition coatings) since Hapke's space weathering methods do not work for opaques. This assumption should have only a minor affect on the modeling as we are mixing its spectral properties with the spectral properties of a mature mare soil, and it is the silicates in the soil that exhibit the largest spectral changes with response to space weathering, however the true spectral changes of space weathering ilmenite are unknown (see more in-depth discussion below). We are attempting to measure the spectral effects of space weathering on ilmenite, but these results are too preliminary to use in the modeling at this time.

Reflectance of these two end member mixtures is inverted to single scattering albedo using equation 37 of Hapke (1981). The single particle phase function of the lunar soil is estimated from the mean of the phase coefficients for silicates computed by Mustard and Pieters (1989), and the single particle phase function for ilmenite is that measured by Mustard and Pieters (1989) for magnetite (both being highly opaque oxides). In our modeling we assume the lunar soil has an optically effective grain size of 15 μm, the mean of the size range that Pieters et al. (1993, 2002) found to be optically dominant and the 50% mass fraction in particle sizes measured by Hapke et al. (1970). First, the reflectance data are converted to single scattering albedo. We then add the single scattering albedo of the endmembers weighted by their relative abundances and geometric cross sections (which are functions of grain size). The reflectance of the mixtures is then computed from the weighted single scattering albedo. Mixtures were computed over the range of 0 to 9.5 wt.% TiO_2. Each mixture has a corresponding Ti content (from the weight fraction of ilmenite and its stoichiometry) and spectral ratio (Fig. 9).

If we assume that the lunar soil and ilmenite share the same grain size, then ilmenite has too little influence on lunar color to account for the general correlation in Figs. 3 and 4, although it does cause the spectrally red mare soil to become less red. To account for the observed correlation, we reduced the ilmenite grain size to increase its cross sectional area and hence spectral effectiveness (per Hapke, 1981). In doing so, we find that very small grain sizes of ilmenite, as small as one micrometer in some cases, are necessary to allow ilmenite to account for the observed color variations. These smaller sizes are outside the validity of

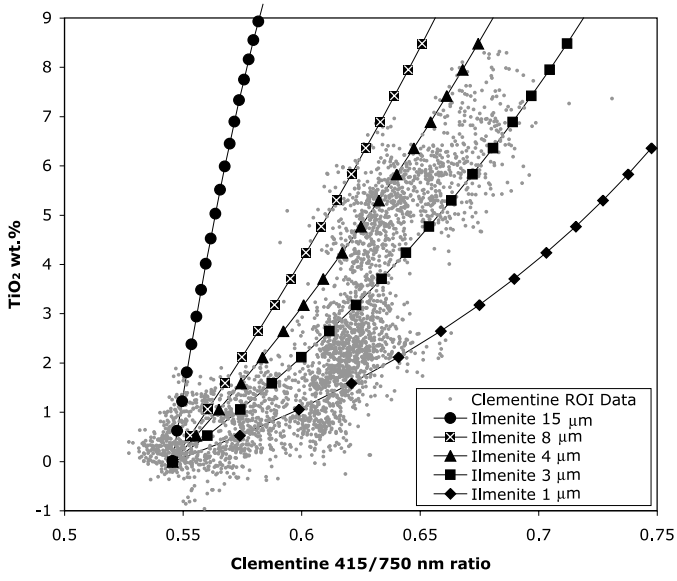

Fig. 9. The affect of ilmenite grain size on the relation between TiO_2 composition and UV–vis ratio, determined using Hapke modelling to calculate UV–vis reflectance as a function of ilmenite grain size for a given TiO_2 content. Ilmenite can produce the observed correlation between UV–vis ratio and TiO_2 composition but only when grain size is very small (<4 μm). Variations in ilmenite grain size could also produce the sigmoidal shape observed in Fig. 2 (gray points represent the ROI data from Fig. 2).

Hapke's model owing to effects of scattering near the wavelength of light. This source of error, however, is compensated by the fact that we did not include the intrinsic darkening that accompanies decreasing grain size of opaques, which would serve to lessen the need to reduce the grain size. The calculated curves are relatively sensitive to the reflectance of ilmenite, and it is possible that lunar ilmenite is darker than the sample used, which would also lessen the need to reduce ilmenite grain size. We anticipate acquiring reflectance measurements of lunar ilmenite separates in the near future.

This modeling suggests that ilmenite can account for the Ti-color relationships observed, but substantial grain size variations are required to account for the observed distribution. If the USGS sample is representative, the ilmenite must have a smaller grain size than the silicates.

One caveat with this model is that it assumes a mature Ti-bearing basalt is equivalent to a mechanical mixture of a mature low-Ti basalt and ilmenite. What this model does not capture is any alteration of the spectral properties of the ilmenite by the ubiquitous vapor deposited coatings present on grains in mature soils that contain nanophase iron and cause spectral reddening, nor the affect of ilmenite on the maturation process. The affect of microcrystalline rims, not amorphous rims, found on ilmenite grains (Keller and McKay, 1997) has not been documented. These rims could conceivably mask the characteristic spectra of ilmenite. Furthermore, a one-to-one correlation does not exist between the bulk TiO_2 composition of the soil and the bulk TiO_2 composition of agglutinates. Using the data of Taylor et al. (2001a) we show that Ti is depleted in agglutinate glasses relative to bulk soil chemistry at high-TiO_2 compositions (Fig. 10), which suggests differential melting of soil constituents during glass formation (Taylor et al., 2001a). Solar-wind irradiation of ilmenite is found to produce preferential removal of Fe and O from the outer few tens of nanometers of ilmenite grains (Christoffersen et al., 1996). This evidence for the resistance of ilmenite to melt and vaporize suggests that ilmenite can contribute to the production of submicroscopic iron but not at the expense of its destruction. This would allow high-Ti basalts to contain two phases of opaques, submicroscopic iron and ilmenite. If it is the submicroscopic iron in the glass that causes reddening than this could explain why high-Ti soils appear redder than expected on the basis of continuing the UV–vis trend of the low-Ti basalts.

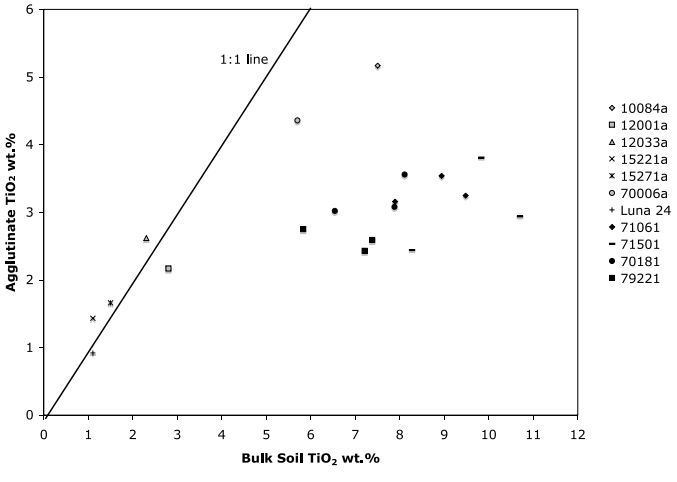

Fig. 10. Comparison of TiO_2 wt.% in agglutinates versus TiO_2 composition of the bulk soil (<1 mm). Data from Walker and Papike (1981) 10084, 12001, 12033, 15221, 15271, 70006; Blanchard et al. (1978) Luna 24 bulk soil; and Hu and Taylor (1978), and Taylor et al. (2001a,b). There is a sizable difference in TiO_2 composition between the bulk soil and agglutinates when bulk soil TiO_2 >3 wt.%.

4.1.1. Petrologic evidence

Ilmenite grain size can vary with sequence of crystallization. Its grain size does vary greatly between low-Ti basalts and high-Ti basalts, as ilmenite forms very late in the crystallization sequence of low-Ti basalts. Even among high-Ti basalts ilmenite grain size varies according to whether the basalt type is poikilitic, ophitic, or subophitic. Ilmenite forms elongate, bladed grains in the subophitic samples, grading into equant, anhedral grains in the ophitic samples (Papike et al., 1998). Apollo 11 high-K basalts, which are poikilitic, tend to be finer grained than the other high-Ti basalts with granular to intersertal textures. The average grain sizes of these basalts range from 0.2 to 0.7 mm (Papike et al., 1998). In contrast the average grain size for high-Ti, low-K basalts, which exhibit subophitic to ophitic textures, range between 0.25 and 1.5 mm (Papike et al., 1998). Variations in ilmenite grain size among high-Ti basalts, if also found to exist in mare soils, could explain differences observed between Apollo 11 and Apollo 17 basalts in the Clementine data.

Hapke modeling supports the concept that variations in ilmenite grain size can affect the UV–vis continuum, with smaller grain size yielding darker spectra (Section 4.1). At this time, however, the measurements of the physical characteristics of ilmenite and their affects on the UV–vis ratio are not known. This hypothesis is testable by means of examining ilmenite grain size of different mare soils using SEM image analysis, for example, and comparing these data with grain sizes predicted from our Hapke modeling.

4.2. Lack of evidence for an observable Fe–Ti charge transfer absorption in the UV

The model by Pieters (1978, 1993) requires that Fe–Ti charge transfers in lunar glasses, which become stronger as Ti in the glass increases, produce a steep absorption between the UV and vis wavelengths; thus, reducing spectral contrast. We tested this hypothesis using Clementine UV–vis ratio and 11-band data, and Hapke modeling of lunar glasses.

To specifically examine the strength of Fe–Ti charge transfer in the UV, we construct a reflectance normalized

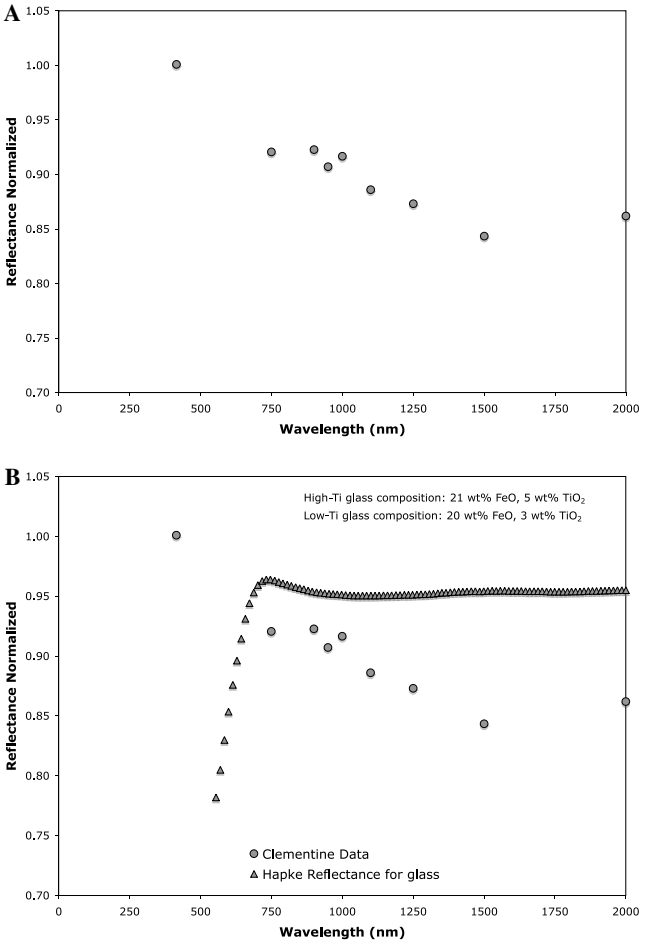

Fig. 11. (A) Clementine UV, vis, and near infrared normalized reflectance data obtained across a flow boundary in Oceanus Procellarum, demarcated by the heavy white line in Fig. 12. The smooth inverse-relation between normalized reflectance and wavelength suggests that an Fe–Ti charge transfer from high-Ti glasses is not a major component of the UV–vis spectrum. The data are an average of three 1×40 pixel regions of interest collected from a 1 km resolution Clementine mosaic. Reflectance normalized values are calculated by dividing average Clementine reflectance values of the low albedo mare with the average Clementine reflectance of the higher albedo mare at each wavelength. (B) Comparison of Hapke modeled reflectance values for Fe + Ti glass using the Bell et al. (1976) absorption coefficients, and Clementine normalized reflectance data. The steep drop-off in normalized reflectance values illustrates effect of the Fe–Ti charge transfer. On this basis, an Fe–Ti charge transfer process in glass is ruled out as a major cause of the color variations in mature mare soils because the Clementine normalized reflectance data smoothly decrease throughout the infrared, not sharp like the Hapke modeled data indicate.

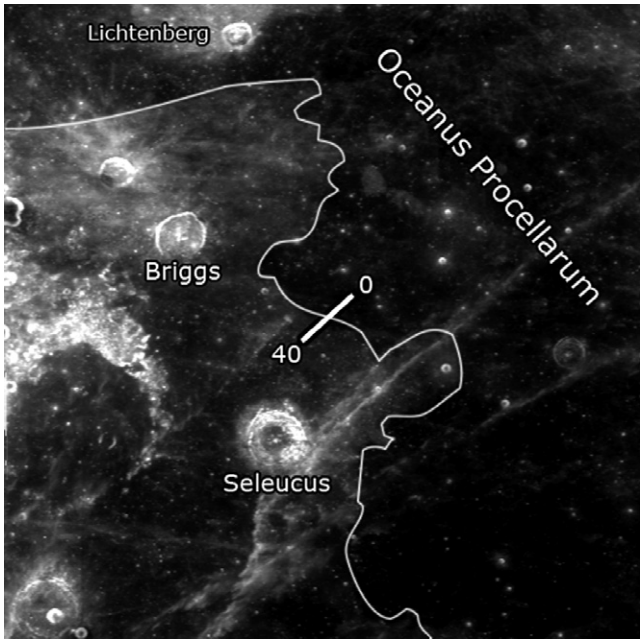

Fig. 12. Clementine 750 nm image showing the cross section location from which data for Fig. 11 were obtained. The thin white line depicts the boundary between the lower-Ti unit (lower left) and higher-Ti unit (upper right). The center of the traverse is at 65 °W; 24 °N.

profile (Fig. 11) for a transect across two adjacent mare units in Fig. 12. Reflectance normalized values are calculated by dividing average Clementine reflectance values of the low albedo mare (composition 21 wt.% FeO, 4.8 wt.% TiO_2) with the average Clementine reflectance of the higher albedo mare (composition 20 wt.% FeO, 2.7 wt.% TiO_2) at each wavelength. Seventeen of the 40 pixels in the mare transect determine the average reflectance values for the brighter, low-Ti mare pixels, and 23 pixels for the darker, higher-Ti mare pixels. Fig. 11 illustrates that, with regards to the UV–vis ratio, the difference in reflectance between the two mare units is much greater at 750 nm than at 415 nm. Specifically, that contrast in reflectance smoothly increases across ratio unit boundaries from approximately 0 percent in the UV, to a strong 15% at 1.5 μm (Fig. 11)—at wavelengths longer than 2 μm contrast is slightly reduced by thermal emission.

As an additional test, we used Hapke modeling to calculate the reflectance values of glasses with similar compositions as the basalt flows in above transect. The grain size of the glass was constrained to 15 μm and the optical constants for Fe–Ti glasses were derived from reported absorption coefficients and compositions of seven synthetic lunar glasses with varying Fe and Ti compositions measured by Bell et al. (1976). The Hapke modeled Fe–Ti glasses clearly show the sharp increase in normalized reflectance values between the UV and vis, which is opposite to the trend observed in the Clementine data (Fig. 11). This disparity between trends precludes the possibility of Fe–Ti charge transfer as the mechanism causing UV–vis color variations in the mare. The Bell et al. (1976) data also reveal that at wavelengths shorter than 700 nm the sum of FeO and TiO_2 governs absorption (Wilcox et al., 2006), while at wavelengths longer than 700 nm the correlation is dominated by FeO alone as noted by Lucey et al. (1995). We can also see from the Bell et al. (1976) data, that if charge transfer was occurring as a result of Ti–Fe-bearing glasses, the glasses would actually appear red, due to the growth of the Fe^{2+}–Ti^{4+} bands (Wells and Hapke, 1977). It is not clear howev-

er, the extent to which the red color of the glass would be masked by space weathering effects (e.g., submicroscopic iron), as these effects are unknown. We are attempting to resolve this question through future experimentation.

In addition, inspection of the Clementine 2.7 μm global mosaic clearly shows unit boundaries within the maria that are also present in the UV–vis ratio images (Fig. 13). The correlation between the 2.7 μm data and the UV–vis ratio is shown in Fig. 14. These data represent all mare pixels with greater than 11 wt.% FeO in the half-degree Lunar Prospector neutron spectrometer data. We then decorrelated these data to determine the spatial distribution of regions where poor correlations exist between the data sets. We did this by regressing the 2.7 μm data on the UV–vis ratio, applying the regression constants to the 2.7 μm data, then differencing the two data sets. Consequently we find, that the spatial distribution is largely random, with some faint indistinct units of low correlation in Mare Frigoris, Mare Fecunditatis, and the Flamsteed region in Oceanus Procellarum (3°S; 44°W). This result suggests that the mechanism that gives rise to spectral differences between mare units operates across the entire UV and near-IR, and is not confined to the UV, ruling out a substantial contribution from Fe–Ti charge transfer absorption that are confined to the UV and blue portion of the visible range (Gillis et al., 2005). In addition, areas where the correlation between 2.7 μm data and the UV–vis ratio is poor hints that the mechanism that produces spectral variations sensed by the UV–vis ratio, does not act uniformly in the near-IR and may indicate areas where charge transfer occurs.

A potential explanation why Fe–Ti bands do not markedly affect lunar mare spectra is that the high-Ti glasses, although ubiquitous in the maria, may occur as agglutinates, which also contain abundant submicroscopic iron, and thus mask the spectral details of the glasses.

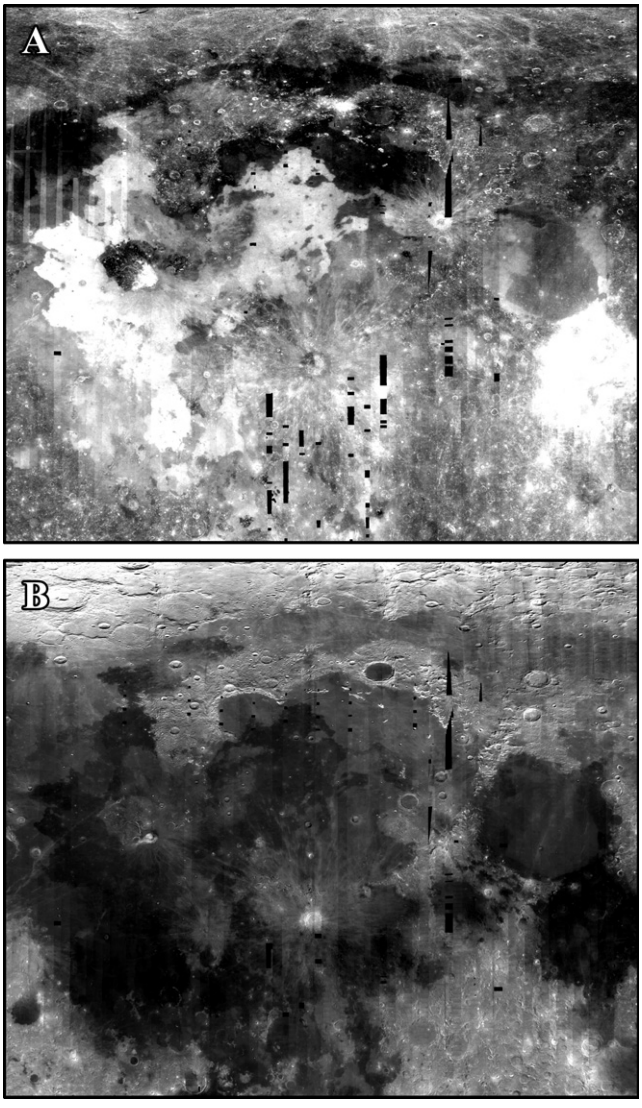

Fig. 13. Two Clementine mosaics centered on the Imbrium-Procellarum region of the Moon: (a) 415/750 and (b) 2780 nm. Bright, high-TiO_2 areas in the ratio image correlate with darkest regions in the 2780 nm data (Fig. 14), which suggest that the mechanism that influences the UV–vis ratio also operates in the near-IR.

4.3. Examining whether the contrast reduction model can account for the UV–vis–TiO_2 correlation

The spectral contrast reduction model (Pieters and McCord, 1976; Pieters, 1993) is incompatible with the

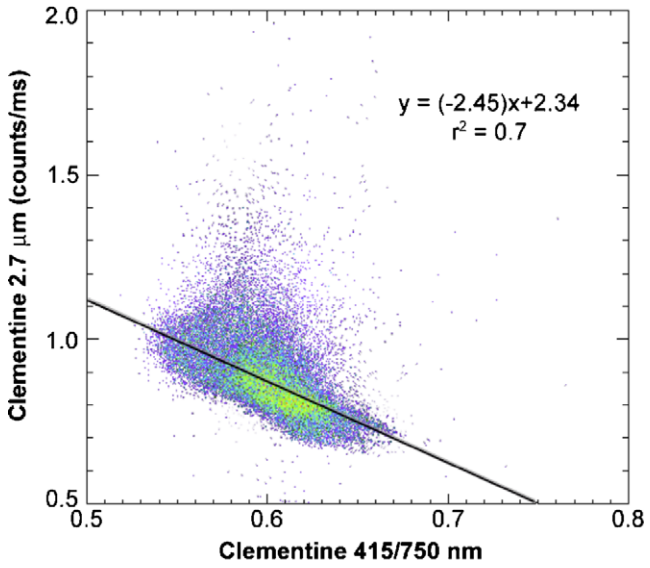

Fig. 14. Clementine 2.7 μm and 415/750 nm reflectance data exhibit a good correlation for all mare areas with >11 wt.% FeO at half-degree resolution. The Clementine 2.7 μm data are provided as calibrated digital numbers (in counts/ms) because they contain both reflectance and thermal emission information. The relation between the UV–vis ratio and near-IR data suggests that UV–vis absorptions for the majority of locations are not due to charge transfer. Fe–Ti charge transfer could still produce UV–vis absorptions for points that lie off the trend.

new data presented here, and with new understanding of the nature of space weathering of high-Ti basalts. The hypothesis was put forward to explain the high correlation of Ti and UV–vis at high Ti, and poor correlation at low Ti. The new data show that color is also variable at high-Ti contents (Fig. 4), undermining the fundamental premise of the model that the ensemble of dark components masks the spectral properties of the individual components and causes uniform color imparted by surface scattering. This hypothesis also contains an explicit assumption that high-Ti soils are qualitatively different from low-Ti soils in a spectral sense, with surface scattering dominating the former and volume scattering dominating the latter. However, new results on space weathering contradict this view. As discussed above, Ti is depleted in agglutinate glass compositions relative to the surrounding mare soil. Furthermore, the lack of a steep positive slope in spectral contrast between the 415 and 750 nm (Fig. 11) precludes darkening by Ti–Fe charge transfer as an explanation of the UV–vis–TiO_2 correlation, and thus agglutinates within high- and low-Ti soils should have similar spectral and scattering properties. In addition, the Clementine data also show that most mare units with high-UV–vis ratios are also distinct at 2.7 μm, so a UV–vis spectral mechanism for causing a soil to become spectrally flatter cannot be dominant (Section 4.2; Fig. 11). As result, we find no evidence that high-Ti soils exhibit a qualitatively different scattering environment than low-Ti soils. What remains fundamentally correct about the contrast reduction model is that mineralogy matters in understanding the UV–visible properties of lunar soils. And as our data reveal, mineralogy matters at all Ti contents, not just low-Ti contents.

5. Controls on the UV–vis slope

5.1. Factors other than ilmenite that may affect the UV–vis ratio

Above we examined the effects of ilmenite on the UV–vis ratio. While ilmenite is the major variable in lunar mare basalts, mare basalts vary in several major mineralogical and geochemical parameters that demonstrably or plausibly affect the UV–vis slope. It cannot be expected that all the permutations of mineralogies that yield a similar TiO_2 (or FeO) content will have the same reflectance or UV–visible ratio (Fig. 15). Partitioning Ti into minerals other than the opaque ilmenite would clearly degrade Ti-color correlations due to ilmenite. Small amounts of Ti can substitute into pyroxene, as in the case of Apollo 11 and 17 basalts. This substitution of Ti into the pyroxene lattice causes the mineral to acquire a pink hue in transmitted light; thus, changing its inherent color. In the clinopyroxene structure Ti^{3+} ions give rise to a Fe–Ti charge-transfer band at 340 nm (Wells and Hapke, 1977), and broad absorption band at 450 nm (Burns, 1993). A decrease and flattening of reflectance values is reported in pyroxenes that have incorporated only fractions of a

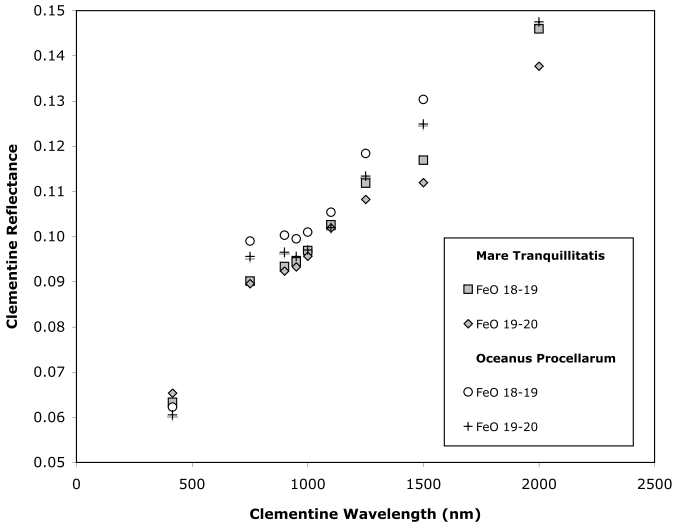

Fig. 15. Basalts in Mare Tranquillitatis Oceanus Procellarum with similar FeO and TiO_2 (5–6 wt.%) compositions (Lunar Prospector neutron spectrometer data) exhibit obvious spectral differences. The Oceanus Procellarum basalts, which are the Eratosthenian flows, exhibit brighter reflectance and redder UV–vis continuum than the Mare Tranquillitatis basalts. The Eratosthenian basalts may contain a greater modal abundance of olivine than the Mare Tranquillitatis basalts, which could produce the difference in reflectance. Such a scenario could explain reflectance differences between Apollo 11 and Apollo 17 basalts, the latter of which contains a higher modal abundance of olivine (Papike and Vaniman, 1978; Papike et al., 1982).

weight percent of TiO_2 (Adams, 1974; Cloutis, 2002). The spectrum of a Ti-rich pyroxene, however, would not be as flat as an ilmenite spectrum. Pyroxenes in Apollo 11 and 17 high-Ti basalts contain TiO_2 concentrations between <1 and 6 wt.%, and even Apollo 12 and 15 pyroxenes contain non-trivial amounts of TiO_2 (<1–4 wt.%) (Papike et al., 1991; Papike et al., 1998). The incorporation of Ti^{4+} and Ti^{3+} into pyroxene is done to maintain charge balance with Al^{3+} as $R^{2+}TiAl_2O_6$ (Bence and Papike, 1972) due to the coprecipitation of augite and plagioclase, and depending on the fO_2 at the time of crystallization. Thus, variations in the sequence of crystallization may yield different reflectance values for basalts with similar bulk chemistries. As TiO_2 content of lunar basalts increases, however, ilmenite becomes the dominant TiO_2-containing phase, which suggests that the UV–vis ratio would only be affected by silicate-bearing TiO_2 phases at low TiO_2 concentrations.

Although a good correlation between total opaques and bulk TiO_2 content of mare basalts has been shown to exist (Lucey et al., 1998), Ti-poor opaques or Ti-free opaques such as chromite ($FeCr_2O_4$) or ulvöspinel ($FeTiO_4$) would affect the UV–vis continuum similar to ilmenite (Riner et al., 2005). The presence of Ti-poor opaques, which are abundant in some basalts (e.g., Papike et al., 1982), would obviously contribute to poor correlations between UV–vis color and Ti as they exhibit similar spectral properties but lower Ti than ilmenite ($FeTiO_3$). This effect would cause the UV–vis spectrum of low-Ti mare basalts to appear rel-

atively blue; thus, their TiO_2 content would be overestimated (e.g., Mare Crisium would be a good candidate for this test). Each weight percent that TiO_2 is overestimated using the UV–vis spectral method can be accounted for by ~1.5 volume percent of non-Ti opaque minerals.

A third factor, the iron content of silicate minerals in basalts and of glasses found in the regolith has a strong control on the visible reflectance that can also contribute to variations in UV–vis ratio. Iron content affects the visible reflectance of all silicate minerals (Adams, 1974; Hazen et al., 1977; Hazen et al., 1978; Cloutis, 2002), the possibility of whether iron affects the UV such as to alter the ratio is discussed in Section 6.3.

Each silicate exhibits different spectral properties for a given FeO content; olivine is brighter at 750 nm than pyroxene at equal FeO content, thus silicate mineralogy is a candidate for influencing the UV–vis ratio. Moreover, if iron is increased for any individual silicate phase, it will yield a soil with a lower visual albedo and, coupled with the inherently low spectral contrast of mature mare soils at UV wavelengths, a potentially flatter UV–vis continuum. Simulated solar wind irradiation experiments indicate a strong correlation between the amount of darkening and Fe content, with high-Fe materials darkening much more than low-Fe ones (Hapke, 2001). The abundance of submicroscopic iron in vapor deposited coatings on grains is proportional to maturity and bulk FeO content (Morris, 1978). Submicroscopic iron is a major absorbing component now known to occur in lunar soils, and a disproportionate distribution of this material could affect the UV–vis ratio. In addition, Fe–Ti charge transfer bands at 340 nm in augite and 340 and 430 nm in Ti-bearing glasses can influence the UV–vis slope, causing it to become more red, unlike adding Ti as ilmenite, which will tend to make the color bluer. Hence, these charge transfer bands cannot cause the Charette relation but could cause scatter in the relation. Potentially more important is how the two spectral processes between Ti in glass and Ti in ilmenite oppose each other, and as a result, make the TiO_2–UV–vis curve steeper and produce the observed sigmoidal shape.

Finally, trace or minor elements (e.g., Cr, V, and Mn), like the major transition elements in mare basalts (e.g., FeO and TiO_2), have strong effects on visible color of silicate minerals (Burns, 1993). The ability of trace elements to influence color could also contribute to poor correlations between Ti and lunar color.

This list of factors that exhibit possible control on the UV–vis ratio serves as a guide for evaluating their effectiveness for influencing the UV–vis–TiO_2 relation. On this premise, we integrate Clementine UV–vis data, Lunar Prospector data, sample mineralogy and mineral chemistry, along with Hapke modelling of mineral spectra for two study areas in the next section in an effort to better characterize the correlation of TiO_2–UV–vis. Integrating these data sets provide information to test spectroscopic models that attempt to explain variations in the UV–vis–TiO_2 correlation.

6. Using sample and remote sensing observations to examine how factors other than ilmenite may affect the UV–vis ratio

6.1. Using mineral and compositional information of basalts in Mare Crisium and Oceanus Procellarum

While ilmenite is the principal cause of the UV–vis–TiO_2 correlation, mineralogy, FeO variations, and space weathering produce complications to the relation. We focus on Mare Crisium and Oceanus Procellarum for further investigation of these mineralogical and compositional influences on the UV–vis ratio discussed above. These two study areas were selected because they occupy the lower and upper trends of Fig. 3, respectively. As a result, mineralogic and/or chemical similarities and differences revealed between these two study areas may help to explain the basis for the offset in UV–vis–TiO_2 trend.

We investigate Mare Crisium as a ground-truth point because it lies off both the trend defined by the Charette Relation and the trend between Clementine UV–vis ratio data and Lunar Prospector TiO_2 data (Fig. 4), and we have sample information. The petrology and mineral chemistry of the Luna 24 samples are distinct for multiple reasons. Soils from Luna 24 contain fragments of ferrobasalt (Papike and Vaniman, 1978), which are relatively low in TiO_2 (~1 wt.%), high in Al_2O_3 (12–14 wt.%), and unusually low in Cr_2O_3 relative to other mare basalts in the sample collection (Laul et al., 1978; Ma et al., 1978). The Luna 24 basalts contain the second lowest modal percentage of opaques of basaltic samples in the lunar collection (1.8%), which is far lower than the basalt types use to calibrate TiO_2 algorithms (Charette et al., 1974; Pieters, 1993; Blewett et al., 1997; e.g., Lucey et al., 2000a; Gillis et al., 2003). Apollo 17 very high-Ti basalts contain up to 24.4% opaques and Apollo 11 low-K basalts contain 14.6%; the lowest modes are Apollo 15 olivine and pigeonite basalts, which contain 5.5 and 3.7% opaques, respectively. The modal percentages are normalized to the sum of four major mineral components (Papike and Vaniman, 1978).

The Eratosthenian aged (Schultz and Spudis, 1983; Wilhelms, 1987; Hiesinger et al., 2003) flows of Oceanus Procellarum are observed to be among the darkest on the Moon (Pohn and Wildey, 1970). Gillis et al. (2003) identified these basalts flows as having the largest errors in predicted TiO_2 concentration, calculated using Clementine spectral reflectance data (Lucey et al., 1998, 2000a) relative to the Lunar Prospector data (Elphic et al., 2002; Prettyman et al., 2006). UV–vis ratio values for Procellarum 1 and 4 ROIs are similar to parts of Mare Tranquillitatis (Figs. 3 and 4), yet reported TiO_2 abundances range from 4 to >10 wt.% depending on the data source and citation. UV–vis-based (e.g., Clementine and Earth-based) calculations yield systematically higher TiO_2 estimates than the Lunar Prospector data sets. For example, titanium compositions reported for these basalts range from a high of >10 wt.% (Pieters et al., 1980; Lucey et al., 2000a), to a moderate 7–10

wt.% (Johnson et al., 1991b; Gillis et al., 2003), and finally to a low of 4–6 wt.% TiO_2 (Elphic et al., 2002; Prettyman et al., 2006). If we take the Lunar Prospector results as truth, than the disparity between color and TiO_2 content is quite striking between the two basalt groups.

Thus, we use sample and remote sensing observations of Mare Crisium and Oceanus Procellarum basalts to examine mineralogical and compositional factors other than ilmenite that may affect the UV–vis ratio.

6.2. Mineralogical and compositional affects on UV–vis color

6.2.1. Olivine

The presence of olivine is expressed in both sample and remote sensing data for Mare Crisium and the Eratosthenian basalts at levels above average for mare basalts. The modal abundance of olivine in the Luna 24 samples (10.4%), second only to the Apollo 12 olivine basalts with 20.2% olivine (Papike and Vaniman, 1978). Apollo 17 contains, at most, 4.6% olivine and Apollo 15 olivine basalts contain 7%. These two locations comprise over half of the ground truth points in the UV–vis TiO_2 calibration of Blewett et al. (1997), Gillis et al. (2003), and Lucey et al. (2000a).

The young Procellarum basalts also exhibit an abundance of olivine similar to or even higher than the Luna 24 basalts. The presence of olivine has been detected in these basalts with remotely sensed data (Pieters et al., 1980; Staid and Pieters, 2001; Lucey, 2004). Preliminary modal abundance estimates suggest that olivine is the dominant mafic phase present in these basalts, ~50% of the mineral assemblage by volume (Lucey, 2004).

However, olivine does not appear to cause the dual trend (Figs. 3 and 4), as its presence occurs in basalts of the upper (Procellarum) and lower trends (Crisium). Nonetheless, the reflectance spectrum of olivine is different than that of pyroxene (Burns, 1993), olivine being brighter and redder than pyroxenes of similar iron contents, and would exert at least some influence on the UV–vis continuum (Fig. 15). Thus, variations in the olivine-to-pyroxene ratio could affect the UV–vis continuum, causing uncertainty in the UV–vis–TiO_2 relation. For example, the TiO_2 values calculated using the equation of Lucey et al. (2000a) were least accurate for areas that are known to contain a high olivine abundance. Therefore it may be necessary to correct spectra for the variable olivine-to-pyroxene ratio. The mineral mapping method of Lucey (2004) will facilitate in this effort. However, before a mineralogic correction can be applied to the UV–vis data, a systematic investigation into the effects of olivine and pyroxene on the UV–vis continuum is necessary, and better optical constants in the UV and visible portion of the spectrum are needed.

6.2.2. Plagioclase

The abundance of plagioclase, either as a primary component of basalt or as a highlands contaminant, as a result of vertical or horizontal impact mixing, can dramatically affect the UV–vis ratio. Feldspathic materials clearly obey a different spectral relationship than the mare materials. Consequently, we find that some of the bluest low-titanium basalt ROIs are relatively elevated in plagioclase, e.g., Mare Nectaris, Crisium, and Fecunditatis. The Luna 24 basalts contain a high modal abundance of plagioclase, 39% (Papike and Vaniman, 1978). The only basalts in the sample collection richer in feldspar abundance are the Luna 16 feldspathic basalts (~40% in the 10–20 μm size fraction (Papike and Vaniman, 1978; Simon et al., 1981)), which are also situated off the UV–vis–TiO_2 approximated Charette trend in Fig. 4, and Apollo 14 high-alumina basalts (43%). Plagioclase in the Crisium samples also tends to be slightly more anorthositic than other basalts An_{73}–An_{98} (Coish and Taylor, 1978; Papike and Vaniman, 1978). Mare Nectaris has a similar TiO_2 composition and UV–vis color as Mare Crisium but a vastly different FeO composition (Table 1). The low FeO composition of Mare Nectaris is likely the result of a thin veneer of highlands material covering its surface from the Theophilus and possibly Cyrillus impacts. ROIs that cluster around the Fecunditatis point (e.g., Mare Nubium, Humorum, Procellarum 2, and Procellarum 6; Fig. 4) may also have elevated plagioclase due to highlands contamination, on the basis of their small size, proximity to large crater rays and location near mare-highland boundaries.

These contamination effects are similar to those observed at the Apollo 17 site. Where highlands/plagioclase mixes with one of two other endmembers: low-Ti basalts, which are red, and high-Ti basalts, which are blue. The highland/plagioclase end member causes low-Ti soils to become bluer without, of course, adding any TiO_2. While on the other hand, the highland/plagioclase end member lowers the TiO_2 composition of high-Ti soils with only a minor changes in the UV–vis color. At the Apollo 17 site, the effects of highland contamination are observed to occur along North (LRV 10 and 11; Stations 6, 7, and 8) and South Massif (LRV 2, 4, 5, and 6; Stations 2 and 3). The Clementine UV–vis ratio data for these locations varies by only a percent while TiO_2 from sample data decreases by an order of magnitude.

Thus, it is possible that deviations from a straight-line trend between TiO_2 and UV–vis could be caused by an enrichment of highlands/plagioclase with low and moderate TiO_2 basalts. This enrichment may be caused by contamination or inherent presence of plagioclase. Either process would pull low-Ti basalts to the right of the straight-line trend (using Sinus Roris and Mare Tranquillitatis as the two end member points), causing them to appear too blue, while high-Ti basalts would maintain similar UV–vis color but be reduced in TiO_2 composition. The reduction in TiO_2 composition with little change in UV–vis ratio for mixing between highlands and high-Ti mare, could also explain the UV–vis difference between Apollo 11 (lower TiO_2) and Apollo 17 (higher TiO_2), which exhibit similar UV–vis color (Table 3).

Therefore it may be necessary to correct spectra for the variable presence of plagioclase. The mineral mapping method of Lucey (2004) will facilitate in this effort. However, before a mineralogic correction can be applied to the UV–vis data, a systematic investigation into the effects of plagioclase on the UV–vis continuum is necessary, and better optical constants in the UV and visible portion of the spectrum are needed.

6.2.3. FeO

Areas that exhibit the biggest errors in predicted TiO_2 coincide with locations that exhibit enriched iron composition. Measured FeO compositions for Mare Crisium, by both sample and remote sensing, are the highest for basalts that comprise the low-TiO_2 trend (Figs. 3 and 4). Samples from Mare Crisium exhibit the highest FeO values of any basalt in the lunar sample collection, at >20 wt.% (Papike and Vaniman, 1978). The Luna 24 olivines are zoned to much more Fe-rich compositions (Fo_{60}–Fo_5) than olivines of Apollo 17 VLT basalt (Fo_{76}–Fo_{53}) and they are more iron-rich on average as well. Pyroxenes in these samples also exhibit similar iron-rich compositions (Fs_{20}–Fs_{80}). Clementine UV–vis-based FeO estimates are consistent with the sample data. In the area surrounding the Luna 24 landing site basalts range from 16.3–20.8 wt.% FeO with an average of 19.2 wt.% FeO.

Also like Mare Crisium, the Eratosthenian flows in Oceanus Procellarum exhibit a poor correlation between UV–vis color and TiO_2 composition, and contain relatively high-Fe concentrations (>21 wt.% FeO (Elphic et al., 2002; Prettyman et al., 2006)). In fact, on the basis of the remote sensing data, the iron composition and olivine content of these basalts appear even more extreme than the Luna 24 soil components. However, returned samples from this location would serve to better quantify these differences and help to determine other important similarities and differences. The high FeO content of Mare Crisium and the Procellarum lava flows could yield a disproportionate influence on the UV–vis reflectance spectra and high-concentrations of submicroscopic iron.

6.3. Disproportionate influence of FeO on UV–vis reflectance spectra

Variations in the bulk soil iron content, whether as submicroscopic iron or high-iron silicates, would have noticeable effects on the UV–vis continuum. For iron in all of its various forms to have no effect on UV–vis color, the effect of Fe reflectance at UV wavelengths would have to be compensated precisely proportional to the variations in the visible (Rava and Hapke, 1987). Thus, it is plausible that reduction in reflectance in the near infrared, caused by submicroscopic iron and increased iron in silicates, coupled with the inherently low spectral contrast of mature mare soils at UV wavelengths yields disproportionately lower reflectance values at 750 nm relative to 415 nm.

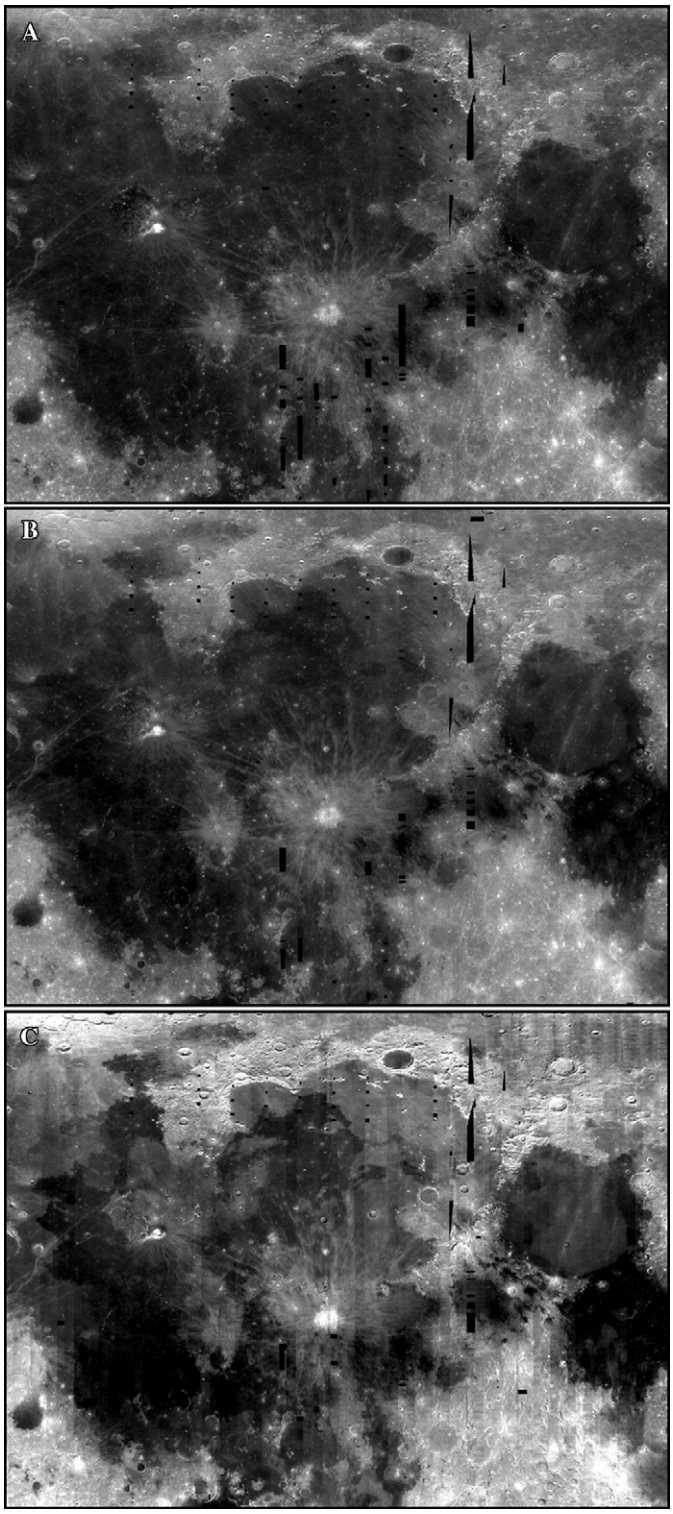

Fig. 16. Three Clementine mosaics of the Imbrium-Procellarum region of the Moon: (A) 415 nm, (B) 750 nm, and (C) 2780 nm. These images illustrate the increase in spectral contrast with increase in wavelength. In addition to the 415/750 nm ratio data, using the 2780 nm data may provide the necessary information for improving the predictability of TiO_2 composition using spectral analysis.

The UV–vis ratio is the focus of this study, but in terms of the component reflectance, the "lever" on the UV–vis ratio is the visible reflectance, not the UV properties. The

converse of this statement is that when mare soils are contaminated by highlands material (e.g., Mare Nectaris) their UV–vis reflectance spectrum becomes bluer as the change in the UV increases faster than the change in the visible wavelengths. UV (415 nm) and vis (750 nm) images of the mare show only minor differences between units; while the longest Clementine wavelength available (2.7 μm) show very high contrast in the mare relative to and data contrast in the mature mare increases with wavelength (Fig. 16). Quantitatively put, the UV portion of the spectrum exhibits 50% less variation as the visible portion of the spectrum and about 75% less variation than at 2000 nm (Fig. 17). Awareness of this fact leads us to the conclusion that any mechanism that can alter the visible reflectance can also alter the UV–vis ratio, provided it influences the UV reflectance to a lesser degree. A corollary is that any mechanism that can alter the visible reflectance is a candidate for control of the UV–vis ratio.

The reflectance of ilmenite at UV wavelengths is similar to mature mare materials and so a greater importance is placed on the visible rather than UV wavelengths. This is evidenced by the fact that the reflectance values of almost all mature mare soils tend to converge towards a single value at 415 nm, likely due to the effects of space weathering (see Section 6.4). As studies of lunar soil reflectance values have established, mature lunar soils exhibit low spectral contrast in the UV portion spectrum (Pieters et al., 1993). Therefore, in addition to TiO_2 content, we propose that the bulk iron content of the soil and mineral chemistry of silicate phases as a mechanism that can alter the visible reflectance and play a direct role in influencing a soil's UV–vis ratio.

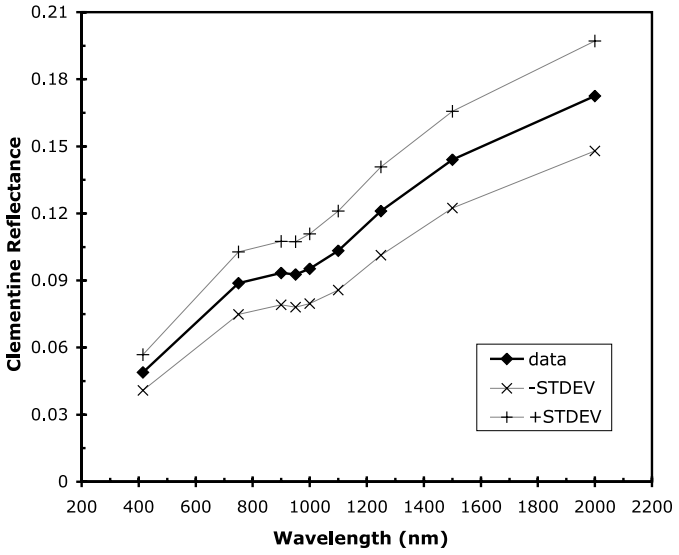

Fig. 17. Clementine 9-band reflectance data averaged for all lunar mare (>11 wt.% FeO). The UV (415 nm) portion of the spectrum exhibits half as much variation as the visible portion of the spectrum (750 nm) and about one quarter as much variation than at 2000 nm. Variations at the longest Clementine wavelength (2780 nm) exhibit even greater variation and are highly correlated with the Clementine 415/750 ratio (Gillis et al., 2005). The 2200 and 2780 nm data are not included in this figure because they are not in units of reflectance.

On the basis of this premise, increasing the FeO content of silicates and agglutinitic glass can yield a flatter UV–vis continuum without the addition of ilmenite (Figs. 18 and 19). In this instance, the UV–vis color is affected by a disproportionate lowering of reflectance at 750 nm relative to 415 nm. In Fig. 18 lines of similar TiO_2 content, thus approximately similar ilmenite content, assuming that increases in FeO are accounted for by other phases, are compared with UV–vis color. To first-order color correlates with TiO_2 composition, as TiO_2 increases for a given FeO content spectra become bluer. However, the UV–vis ratio for a given TiO_2 content varies with FeO composition. For instance, high-Ti basalts (>5.5 wt.%) with <20 wt.% FeO are bluer than basalts of similar TiO_2 composition and higher iron contents. The UV–vis ratio also reacts counter intuitively when TiO_2 is between 1.5 and 4.5 wt.%. UV–vis ratios for low-iron basalts (16.5 wt.% FeO) tend to be spectrally bluer than basalts with slightly higher iron. We suspect that this effect is likely the result of highlands/plagioclase enrichment for these basalts. As discussed previously about Apollo 17 (Section 6.2.2), where highland/plagioclase contamination causes low-Ti soils to become bluer without adding any TiO_2. Lastly, we find that UV–vis color contrast decreases as iron content increases for basalts of all Ti compositions. This finding is similar, but for FeO rather than TiO_2, to the spectral contrast model of Pieters (1978, 1993).

Fig. 19 illustrates how, in general, basalts become bluer as TiO_2 increases. In this plot, lines connect basalts with similar FeO contents. Increases in TiO_2 composition are not accompanied by increases in FeO; thus, it is possible that TiO_2 is not representing an increase in ilmenite content. If the increase in TiO_2 does represent an increase in ilmenite content then FeO must be scavenged from the silicate portion in order to satisfy the ~50:50 mix of the two in ilmenite. Either effect, increasing TiO_2 in non-ilmenite phases or scavenging FeO from other phases, would have direct consequences on the spectral properties of the materials. For basalts with <21 wt.% FeO, UV–vis color correlates almost uniformly with TiO_2 composition. Basalts with >21 wt.% FeO, however, exhibit a noticeably flatter trend. At low-Ti concentrations the high-iron basalts are bluer than basalts of similar TiO_2 content but lower iron. As TiO_2 increases in these high-iron basalts, they become spectrally redder than basalts of similar TiO_2 compositions but lower iron. This evidence suggests that iron lowers spectral contrast of mare basalts, as observed in Fig. 18. In fact, data for all high-Ti soils, regardless of FeO composition, suggests the trend is to become spectrally redder, rather than bluer, as FeO content increases. This is interestingly not the case in Fig. 18, where higher-Ti, high-Fe basalts are still bluer than their lower-Ti, high-Fe complement. The potential for removing/reducing the spectral effects of FeO are evidenced in Fig. 19. The slope of the higher-iron basalts (>21 wt.% FeO) can be adjusted to match

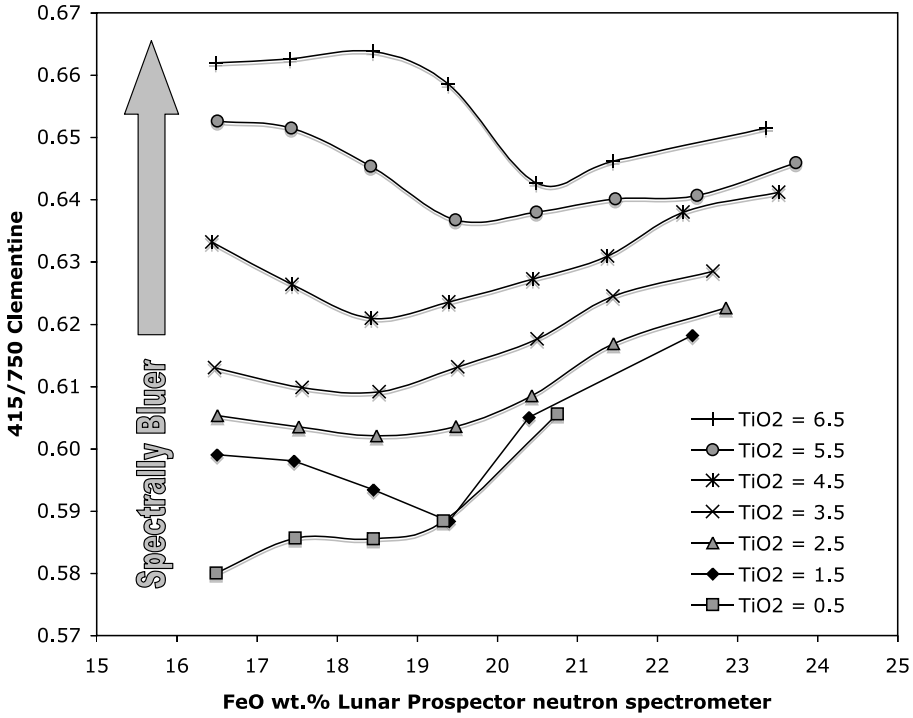

Fig. 18. Globally averaged 415/750 nm and FeO data are compared for basalt units separated by FeO and TiO_2 in 1 wt.% increments (Lunar Prospector neutron spectrometer data). For example, compositions labeled 17.5 wt.% FeO and 1.5 wt.% TiO_2 represents all basalts with a surface composition between 17–18 wt.% FeO and 1–2 wt.% TiO_2. Lines connect basalt units of similar TiO_2 composition and possibly similar ilmenite content. This plot and Fig. 19 endeavor to separate the effects of FeO and TiO_2 on UV–vis ratio. We observe that lower FeO basalts (16–18 wt.%) are relatively blue compared basalts of similar TiO_2 and slightly higher FeO compositions (18–20 wt.%). This effect is likely the result of highlands/plagioclase enrichment for basalts with <3.5 wt.% TiO_2. Above this level, basalts like Mare Tranquillitatis are inherently bluer than basalts like the Eratosthenian flows in Oceanus Procellarum with similar TiO_2 and higher FeO compositions (Fig. 15). Also, observed is a correlation between 415/750 nm and FeO content of mare basalts. As FeO composition increases from 19 through 24 wt.% the UV–vis ratio also increases. Typically, the highest iron basalt of any TiO_2 trend is bluer than the lowest iron point, however, this is not the case for basalts with >5 wt.% TiO_2. These high-Ti basalts with 16–19 wt.% FeO are mostly contained within Mare Tranquillitatis.

the UV–vis ratio trend of the lower-iron basalt by doing an axis rotation. This modification presents an encouraging possibility for prediction of TiO_2 from color, as it would allow the higher-iron basalts to be characterized by the same algorithms used to estimate TiO_2 on the basis of color for lower-FeO basalts.

As result, variations in mare FeO content lower the correlation between UV–vis ratio and TiO_2 content of mare basalts. In addition, areas that exhibit enriched iron compositions coincide with regions of the biggest predicted TiO_2 errors mapped globally (Gillis et al., 2003). This outcome is observed for Mare Crisium and the Eratosthenian flows in Oceanus Procellarum, where the disproportionate lowering of the visible reflectance relative to the UV due to iron results in an overestimation of TiO_2 contents using the Clementine UV–vis data. The influence of FeO on UV–vis slope may provide the offset correction necessary for increasing the accuracy of UV–vis-based algorithms for estimating TiO_2 abundances. This effort is made complex by the fact that, while the FeO content of mare materials exhibits influence over the reflectance values in the UV, visible, and near infrared portions of the spectrum, the spectral properties of each mare component are different for a given FeO content than all of the other soil components. Although we find that FeO causes a disproportionate lowering of the visible reflectance relative to the UV, this phenomenon does not explain the nature of the dual trend between UV–vis ratio and TiO_2, as data for Crisium basalts lie on the lower trend and data for Procellarum basalts on the upper trend. On this basis, the intrinsic and variable color properties resulting from varying iron content and modal mineralogy yield the observed scatter in the UV–vis–TiO_2 trend, similar to the hypothesis of Pieters (1993).

6.4. Possibility of space weathering products affecting UV–vis color

The lunar surface undergoes physical and chemical changes as the result of space weathering, which is the exposure to micrometeorite impacts (vapor deposit), solar wind and cosmic ray irradiation (sputtering), and solar wind implantation. The maturity of a regolith is the degree to which it has accumulated these changes; the longer a sample is exposed, the more mature it becomes (McKay et al., 1991). The major products of space weathering, agglutinatic glass and submicroscopic iron (also known

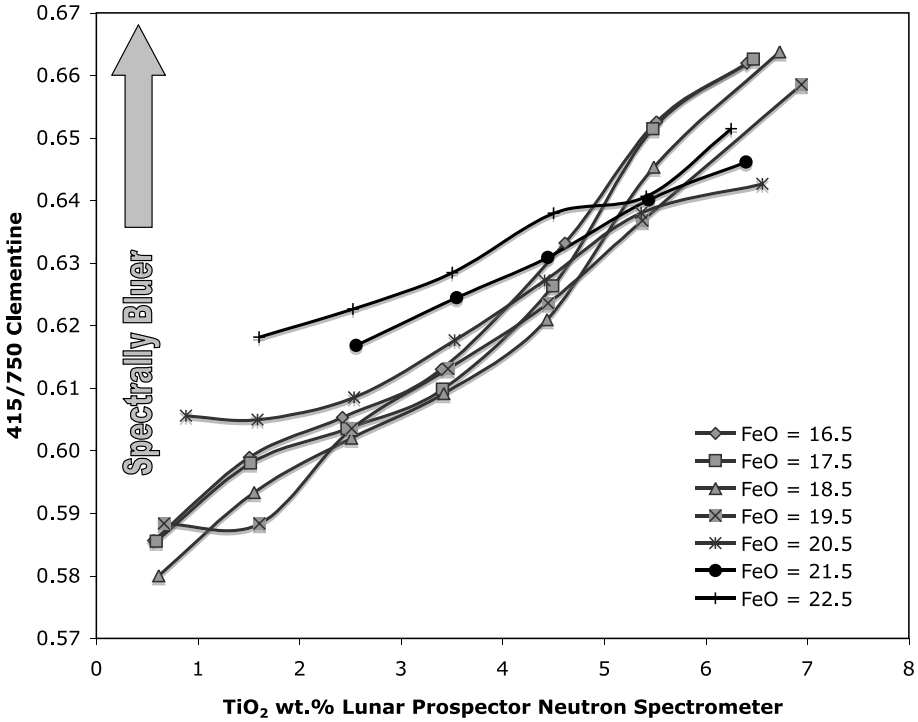

Fig. 19. Global averages of spectral (415/750 nm) and compositional data for basaltic soils. Basalts are grouped by FeO and TiO_2 into 1 wt.% increments as in Fig. 18. Lines connect basalt units of similar FeO composition. Mare basalts with <21.5 wt.% FeO tend to follow a single UV–vis ratio trend, while basalts with higher FeO compositions exhibit a shallower UV–vis ratio trend. The shallower trend supports why low-Ti, high-FeO basalts are bluer than their lower-FeO counterparts, and why the high-Ti, high-FeO basalts are redder than their lower-FeO equivalent.

as nanophase iron, abbreviated npFe^0), alter a soil reflectance spectrum (Adams and McCord, 1971; Fischer and Pieters, 1994, 1996), causing darkening, reducing the strength of mineralogical absorption bands, and producing a redder spectral slope. Comminution is the only impact process that acts against space weathering, producing fresh crystalline soils with low glass contents, which causes them to appear brighter and spectrally bluer.

Submicroscopic metallic iron particles occur in thin amorphous rims surrounding individual grains (Keller and McKay, 1993), and as inclusions in agglutinates, the most prevalent weathering product. The submicroscopic iron particles found in thin amorphous mineral coatings are about ~3 nm diameter (Keller and Clemett, 2001). On the other hand, agglutinates, which are fused soil aggregates, contain submicroscopic iron particles that are twice as large (~7 nm in diameter) as the submicroscopic iron found the patina coatings (Keller and Clemett, 2001). Agglutinates are also voluminous, comprising 50% or more of mature soils (McKay et al., 1991).

The primary cause of spectral alteration of the visible and near infrared spectrum of lunar soils is nanophase iron particles. The smaller (<5 nm) submicroscopic iron included in surface coatings largely cause reddening, while the large nanophase Fe^0 particles (>5 nm) typically found in agglutinates result in darkening of the soil (Hapke, 2001). Thus, compositional differences within the soil that could control the production of nanophase iron and/or agglutinates would greatly influence the UV–vis continuum, as demonstrated by strong anomalies exhibited by fresh craters and other immature features.

Morris (1978) showed that the abundance of submicroscopic iron is controlled by the bulk iron content of a soil and its maturity. The more FeO that is available in the soil, the more nanophase iron produced through the weathering process. This is why in order to compare maturities from one soil to the next regardless of iron content, I_s values, which are a measure of the amount of nanophase iron present in a soil, are normalized to FeO content (Morris, 1978). Bulk iron contents of the lunar maria vary by almost a factor of two (Lawrence et al., 2002; Gillis et al., 2004). Therefore, submicroscopic iron contents must also vary by a factor of two. Moreover, areas of enriched iron are found to coincide with regions of the biggest predicted TiO_2 errors mapped globally (Gillis et al., 2003).

The increase in submicroscopic iron may also cause disproportionate reddening of the soil, which could explain the difference in slope between the upper and lower trends in Figs. 3 and 4. Analysis by Hapke (2001) and Noble et al. (2001), indicate increased amounts of nanophase iron or maturity would result in increased reddening to a point, wherein the most mature mare become slightly less red. In this model an increase of submicroscopic iron produces a strong absorption in the UV region, such that only light reflected from the grain surfaces contributes to the UV spectrum, but reflectance at longer wavelengths (>1.5 μm)

is less affected because the long wavelengths are not strongly absorbing. As more submicroscopic iron accumulates beyond a mass fraction of ~0.5% Fe (Noble et al., 2001), even the longer wavelengths become affected as Fresnel reflection (i.e., reflection is controlled by difference in the refractive index between two media as opposed to absorption properties of the material) begins to control reflectance (Hapke, 2001), causing the continuum to approximate a straight line. This flattened spectrum could account for the correlation between the 2.7 μm and 415/750 nm ratio data (Figs. 13 and 14). The enrichment of submicroscopic iron, in higher iron mare, could produce a high 415/750 and low 2.7 μm reflectance value by simultaneously reducing reflectance across the UV, vis, and near-IR wavelengths. In addition, the increased submicroscopic iron would also cause a shallowing of the 1-micron mafic absorption and, as a result, could also explain why the method for calculating FeO by Lucey et al. (2000a) underestimates the high-iron content of the Eratosthenian flows in Procellarum.

It is not clear whether differences in space weathering products could result in the dual UV–vis–TiO_2 trend. Soils of the upper trend (>1 wt.% TiO_2) could appear redder than anticipated, relative to a continuation of the UV–vis ratio trend of the low-TiO_2 basalts, because of greater submicroscopic iron production in patina rims in high iron (Fe + Ti > 18.5) basalts. On the other hand, spectra of low-Ti, high-iron basalts (e.g., Mare Crisium), which contain low amounts of igneous opaque phases, may become dominated by submicroscopic iron and agglutinates. A compositionally linked maturity model could explain why Apollo 11 is darker than Apollo 17 soils, because the I_s/FeO determined for representative soils from the Apollo 11 landing site are more mature than representative soils from the Apollo 17 landing site or mare sample stations (Table 3). Using an optical maturity index parameter, such as the one by Lucey et al. (2000b), could help correct for a soil's degree of maturity. Although the Lucey method for estimating TiO_2 does have the capability to correct for differences in FeO and maturity (Lucey et al., 2000a), it does not accurately estimate the TiO_2 composition of the Apollo 11 landing site.

Another component of space weathering may differentially affect the UV–vis continuum of high-Ti relative to low-Ti basalts. Keller and McKay (1997) showed that microcrystalline rims formed around ilmenite grains and Bernatowicz et al. (1994) described ilmenite surfaces covered by vapor deposits. It has not been determined whether these rims would mask, even to a small extent, the characteristic spectra of ilmenite. If microcrystalline or amorphous rims can shift the UV–vis ratio of ilmenite towards redder or steeper values, then this effect would account for the sigmoidal nature in the UV–vis–TiO_2 trend (Figs. 3 and 4). High-Ti basalts would be relatively less blue than predicted on the basis of low-Ti basalts because of change in the surface nature of the ilmenite grains.

Conclusions about the composition of lunar soils using visible-near infrared spectroscopy must assume that variations in space weathering products are primarily the result of maturation and not composition. This idea is similar to the inference that remotely sensed compositions of the regolith represent the compositions of the underlying bedrock, however, the effort needed to fully understand the interconnectedness between composition, space weathering, and reflectance spectra has only begun (Lucey et al., 2000a; Taylor et al., 2001b; Pieters et al., 2002). Therefore further analyses are needed to understand how soil composition can affect products of space weathering, and how space weathering disproportionately operates on silicate and oxide mineralogy so that these effects on UV–vis spectra can be interpreted and removed.

7. Conclusions

Our comparison of Clementine UV–vis ratio and Lunar Prospector TiO_2 data for 18 individual regions of interest that exhibit uniform color, reveals that the UV–vis–TiO_2 trend is best characterized by a sigmoidal trend (Figs. 3 and 4). The sigmoidal nature of this UV–vis–TiO_2 correlation is notably different than single curvilinear trend of Charette et al. (1974) or Pieters (1993). We divide the sigmoidal structure into two trends on the basis of the relation between UV–vis ratio and TiO_2 composition. The lower slope of the trend is comprised of basalts with <1.5 wt.% TiO_2 or that FeO + TiO_2 sum to ⩽18.5%, while basalts with >1.5 wt.% TiO_2 or the sum FeO + TiO_2 ⩾ 18.5%, occupy the middle and upper trend (Table 1).

The data presented herein invalidate two elements of the spectral contrast reduction model: that charge transfer of Fe–Ti-rich glasses produce flattening of the UV–vis continuum, and that opaque phases mask the spectral properties of the individual components and cause uniform color imparted by surface scattering. First, the Ti composition of agglutinates is depleted relative to the bulk soil Ti composition (Fig. 10). In addition, both Clementine data and lab data confirm the lack of an observable Ti–Fe charge transfer influencing the lunar spectrum (Fig. 11). Third, the UV–vis data we present show that color is variable at low-, medium-, and high-Ti contents (Figs. 3 and 4), which undermines the concept that by increasing the abundance of opaque phases a reduction in spectral contrast results (e.g., Fig. 1). Lastly, the Clementine UV–vis-NIR data also show that mare units with high UV–vis ratios are distinct throughout the infrared (Figs. 13 and 14), so a UV–vis spectral mechanism cannot be dominant. What remains fundamentally correct about this model is that mineralogy matters in understanding the UV–vis properties of lunar soils, and as the data presented here indicate, mineralogy probably matters at all Ti contents, not just low-Ti contents.

Ilmenite remains a leading candidate for controlling the UV–vis–TiO_2 correlation (Figs. 9 and 18). The UV–vis ratio, however, is a measure of the sum of all spectral prop-

erties of all observed minerals and space weathering products. The data presented in this study provide evidence that suggests that other factors play a roll, albeit a secondary one, in influencing color (Figs. 18 and 19). Factors such as iron content in silicates, olivine-to-pyroxene ratio, plagioclase content, ilmenite grain size, and space weathering cause scatter in the UV–vis–TiO_2 correlation; thus, lowering the predictability of TiO_2 from color.

We identify three components within basaltic soils that appear to preferentially produce the sigmoidal UV–vis–TiO_2 trend. (1) The addition of plagioclase either as a contaminant or as an inherent component produces one-of-two results depending on the basalt type in which it is combined. Either it causes the UV–vis ratio of low-Ti basalts to appear bluer than a low-Ti basalt with little plagioclase, or it reduces the amount of TiO_2 of a high-Ti soil while causing a negligible change in the soil's original UV–vis ratio. (2) Formation of amorphous and/or microcrystalline rims around ilmenite grains. These products of space weathering may mask the characteristic spectrum of ilmenite and cause them to appear spectrally redder. (3) Variations in ilmenite grain size resulting from the sequence of crystallization. The finer grain size of a late crystallizing ilmenite in a low-Ti magma would result in a bluer spectrum than a larger ilmenite grain from an early crystallizing ilmenite in a high-Ti magma. (4) Enriched bulk-iron contents appear to have a dual mechanism of controlling the UV–vis ratio by darkening both the mineral phases and agglutinatic glass, and providing more submicroscopic iron within the mature regolith. We suggest that the bulk-iron content has an affect on the UV–vis ratio by disproportionately reducing reflectance at 750 nm relative to 415 nm (Figs. 17 and 19). As a result, a flatter UV–vis continuum is produced with increased iron alone. Potentially more important is how the two spectral processes between Ti in glass, which causes reddening, and Ti in ilmenite, which causes material to become more blue, oppose each other, and as a result, make the TiO_2–UV–vis curve steeper and produce the observed sigmoidal shape.

We find evidence for two mechanisms that can yield UV–vis variations without producing the sigmoidal UV–vis–TiO_2 trend. (1) Variations in the olivine-to-pyroxene ratio affect the UV–vis spectrum of basalts because olivine for a given iron content is brighter and redder than pyroxene (Fig. 15). (2) Pyroxene with a moderate TiO_2 content can also produce a darker flatter UV–vis spectrum.

One result of the sigmoidal UV–vis–TiO_2 trend is that units with intermediate color, between 0.58 and 0.66, have the highest uncertainty with respect to predicting TiO_2 (Figs. 3 and 4). Our finding is in contrast to previous work, which portrayed the largest variations in titanium occurring with low UV–vis ratio values. It also brings to light that TiO_2 compositions of a large portion of the maria are not known with great confidence because basalts of intermediate color cover seventy-five percent of the mare surface area (Fig. 5). This outcome has implication on estimates of the bulk composition of the Moon and resource assessments that intend to utilize ilmenite.

Five key observations are revealed from Figs. 18 and 19: (1) that the UV–vis ratio increases as TiO_2 increases and FeO is held constant. (2) The UV–vis ratio decreases as FeO increases and TiO_2 is held constant for basalts >5.5 wt.% TiO_2—basalt units between 1.4 and 4.5 wt.% TiO_2 at first become spectrally redder but then become spectrally bluer as FeO increases. (3) Spectral contrast is reduced for all mare basalts as FeO increases above 20 wt.%. (4) For basalts with <21 wt.% FeO, UV–vis color correlates almost uniformly with TiO_2 composition, however, basalts with >21 wt.% FeO exhibit a noticeably flatter trend. (5) The potential for removing/reducing the spectral effects of FeO are possible by doing an axis rotation. This adjustment allows for the possibility of improving the prediction of TiO_2 from color, as it would allow the higher-iron basalts to be characterized by the same algorithms used to estimate TiO_2 on the basis of color for lower-FeO basalts.

Additional information is needed to further refine the dual TiO_2 trend. For example, Hapke modeling of mineral spectra is currently limited by the lack of optical property measurements of olivine, pyroxene, and ilmenite in the UV–vis region. Thus, additional measurements of these minerals with varying composition are necessary in order to overcome this hurdle. For instance, the spectral contribution by Ti-bearing silicates to the UV–vis ratio cannot be quantified using radiative transfer modeling at this time. Future analysis of Earth-based 70-cm radar data (e.g., Thompson, 1987; Campbell et al., 1997), which is sensitive to ilmenite phases but not titanium bearing silicates, will play in important role in evaluating the presence of Ti enriched silicates.

In this analysis we attempt to increase understanding of the relationship between color and TiO_2 in order to map Ti content of the lunar maria with high fidelity. Improving the concordance between these two parameters will also prove useful interpreting data from upcoming remote sensing missions to the Moon. In addition, future mission data with higher spectral and spatial resolution, and addition analytical instruments will also further our understanding of the composition of the lunar regolith (e.g., SMART-1, SELENE, Chandrayan-1, Chang'e-1, and Lunar Reconnaissance Orbiter).

Acknowledgments

We thank Bruce Hapke, Aileen Yingst, Brett Wilcox, and AE Christian Koeberl for helpful reviews that served to improve the manuscript. We also thank Bruce Hapke for suggesting the construction of Fig. 19. This work was supported by NASA Grant NNG05GJ34G.

Associate editor: Christian Koeberl

References

Adams, J.B., 1974. Visible and near-infrared diffuse reflectance spectra of pyroxenes as applied to remote sensing of solid objects in the solar system. *J. Geophys. Res.*, 4829–4836.

Adams, J.B., McCord, T.B., 1971. Alteration of lunar optical properties: age and composition effects. *Science* **171**, 567–571.

Bell, P.M., Mao, H.K., Weeks, R.A., 1976. Optical spectra and electron paramagnetic resonance of lunar and synthetic glasses: a study of the effects of controlled atmosphere, composition, and temperature. In: *Proc. Lunar Sci. Conf. 7th*, 2543–2559.

Bence, A.E., Papike, J.J., 1972. Pyroxenes as recorders of lunar basalt petrogenesis: chemical trends due to crystal–liquid interaction. In: *Proc. Lunar Sci. Conf. 3rd*, 431–469.

Bernatowicz, T.J., Nichols Jr., R.H., Hohenberg, C.M., 1994. Vapor deposits in the lunar regolith. *Science* **264**, 1779–1780.

Binder, A.B., 1998. Lunar Prospector: overview. *Science* **281**, 1475–1476.

Blanchard, D.P., Brannon, J.C., Aaboe, E., Budahn, J.R., 1978. Major and trace element chemistry of Luna 24 samples from Mare Crisium. In: Merrill, R.B., Papike, J.J. (Eds.), *Mare Crisium: The View from Luna 24*. Pergamon Press, pp. 613–630.

Blewett, D.T., Lucey, P.G., Hawke, B.R., Jolliff, B.L., 1997. Clementine images of the lunar sample-return stations: refinement of FeO and TiO_2 mapping techniques. *J. Geophys. Res.* **102**, 16,319–16,325.

Burns, R.G., 1993. *Mineralogical Applications of Crystal Field Theory*. Cambridge University Press, Cambridge [England]; New York, NY, USA.

Burns, R.G., Parkin, K.M., Loeffler, B.M., Leung, I.S., Abu-Eid, R.M., 1976. Further characterization of spectral features attributable to titanium on the Moon. In: *Proc. Lunar Conf. 7th*, 2651–2578.

Campbell, B.A., Hawke, B.R., Thompson, T.W., 1997. Regolith composition and structure in the lunar maria: results of long-wavelength radar studies. *J. Geophys. Res.* **102** (E8), 19,307–19,320.

Charette, M.P., McCord, T.B., Pieters, C.M., Adams, J.B., 1974. Application of remote spectral reflectance measurements to lunar geology classification and determination of titanium content of lunar soils. *J. Geophys. Res.* **79** (11), 1605–1613.

Christoffersen, R., Keller, L.P., McKay, D.S., 1996. Microstructure, chemistry, and origin of grain rims on ilmenite from the lunar soil finest fraction. *Meteorit. Planet. Sci.* **31**, 835–848.

Cloutis, E.A., 2002. Pyroxene reflectance spectra: minor absorption bands and effects of elemental substitutions. *J. Geophys. Res.* **107** (E6). doi:10.1029/2001JE001587.

Coish, R.A., Taylor, L.A., 1978. Mineralogy and Petrology of basaltic fragments from the Luna 24 drill core. In: Merrill, R.B., Papike, J.J. (Eds.), *Mare Crisium: The view from Luna 24*. Pergamon Press, New York, pp. 403–417.

Dymek, R.F., Albee, A.L., Chodos, A.A., 1975. Comparative mineralogy and petrology of Apollo 17 mare basalts: samples 70215, 71055, 74255, and 75055. In: *Proc. Lunar Sci. Conf. 6th*, 49–77.

Eliason, E.M., Isbell, C., Lee, E., Becker, T., Gaddis, L., McEwen, A., Robinson, M.S., 1999. Mission to the Moon: The Clementine UV–vis Global Images. 78 CD-ROM set produced by the U.S. Geol. Surv., Flagstaff, AZ.

Elphic, R.C., Lawrence, D.J., Feldman, W.C., Barraclough, B.L., Maurice, S., Binder, A.B., Lucey, P.G., 2000. Lunar rare earth element distribution and ramifications for FeO and TiO_2: Lunar Prospector neutron spectrometer observations. *J. Geophys. Res.* **105** (E8), 20,333–20,345.

Elphic, R.C., Lawrence, D.J., Feldman, W.C., Barraclough, B.L., Maurice, S., Lucey, P.G., Blewett, D.T., Binder, A.B., 2002. The Lunar Prospector neutron spectrometer constraints on TiO_2. *J. Geophys. Res.* **107** (E4). doi:10.1029/2000JE001460.

Fischer, E.M., Pieters, C.M., 1994. Remote determination of exposure degree and iron concentration of lunar soils using vis-NIR spectroscopic methods. *Icarus* **111**, 475–488.

Fischer, E.M., Pieters, C.M., 1996. Composition and exposure age of the Apollo 16 Cayley and Descartes regions from Clementine data: normalizing the optical effects of space weathering. *J. Geophys. Res.* **101** (E1), 2225–2234.

Giguere, T.A., Taylor, G.J., Hawke, B.R., Lucey, P.G., 2000. The titanium contents of lunar mare basalts. *Meteorit. Planet. Sci.* **35** (1), 193–200.

Gillis, J.J., Lucey, P.G., 2004. Is random noise causing a poor correlation between the Lunar Prospector TiO_2 data and the Clementine UV–vis-color ratio? In: Nardell, C.A., Yee, J.-H., Garvin, J.B., Lucey, P.G. (Eds.), *Instruments, Science, and Methods for Geospace and Planetary Remote Sensing*. SPIE, Bellingham, WA, 2005, pp. 191–195.

Gillis, J.J., Jolliff, B.L., Elphic, R.C., 2003. A revised algorithm for calculation TiO_2 concentrations from Clementine UV–vis data: a synthesis of rock, soil, and remotely sensed TiO_2 concentrations. *J. Geophys. Res.* **108** (E2), 5009. doi:10.1029/2001JE001515.

Gillis, J.J., Jolliff, B.J., Korotev, R.L., 2004. Lunar surface geochemistry: global concentrations of Th, K, and FeO as derived from Lunar Prospector and Clementine data. *Geochim. Cosmochim. Acta* **68** (18), 3791–3805.

Gillis, J.J., Lucey, P.G., Campbell, B.A., Hawke, B.R., 2005. Clementine 2.7 micron Data and 70-cm Earth-based Radar Data Provide additional constraints for UV–vis-based Estimates of TiO_2 Content for Lunar Mare Basalts. *Lunar and Planetary Science XXXVI*, Lunar Planet. Inst., Houston. #2254 (abstract), CD-ROM.

Hapke, B., 1981. Bidirectional reflectance spectroscopy 1. Theory. *J. Geophys. Res.* **86** (B4), 3039–3054.

Hapke, B., 2001. Space weathering from Mercury to the asteroid belt. *J. Geophys. Res.* **106** (E5), 10,039–10,073.

Hapke, B., Cohen, A., Cassidy, W., Wells, E., 1970. Solar radiation effects of the optical properties of Apollo 11 lunar samples. *Proc. Apollo 11 lunar Science Conf.*, 2199–2212.

Hazen, R.M., Mao, H.K., Bell, P.M., 1977. Effects of compositional variation on absorption spectra of lunar olivines. In: *Proc. Lunar Sci. Conf. 8th*, 1081–1090.

Hazen, R.M., Bell, P.M., Mao, H.K., 1978. Effects of compositional variation on absorption spectra of lunar pyroxenes. In: *Proc. Lunar Sci. Conf. 9th*, 2919–2934.

Hiesinger, H., Head III., J.W., Wolf, U., Jaumann, R., Neukum, G., 2003. Ages and stratigraphy of mare basalts in Oceanus Procellarum, Mare Nubium, Mare Cognitum, and Mare Insularum. *J. Geophys. Res.* **108** (E7), 5065. doi:10.1029/2002JE001985.

Hu, H.-N., Taylor, L.A., 1978. Soils from Mare Crisium: agglutinitic glass chemistry and soil development. In: Merrill, R.B., Papike, J.J. (Eds.), *Mare Crisium: The view from Luna 24*. Pergamon Press, pp. 291–302.

Johnson, J.R., Larson, S.M., Singer, R.B., 1991a. A reevaluation of spectral ratios for lunar mare TiO_2 mapping. *Geophys. Res. Lett.* **18** (11), 2153–2156.

Johnson, J.R., Larson, S.M., Singer, R.B., 1991b. Remote sensing of potential lunar resources, 1. Near-side compositional properties. *J. Geophys. Res.* **96** (E3), 18,861–18,882.

Johnson, T.V., Saunders, R.S., Matson, D.L., Mosher, J.A., 1977. A TiO_2 abundance map for the northern maria. In: *Proc. Lunar. Sci. Conf. 8th*, 1029–1036.

Jolliff, B.L., 1999. Clementine UV–vis multispectral data and the Apollo 17 landing site: What can we tell and how well? *J. Geophys. Res.* **104** (E6), 14,123–14,148.

Keller, L.P., Clemett, S.J., 2001. Formation of nanophase iron in the lunar regolith. *Lunar and Planetary Science XXXII*, Lunar Planet. Inst., Houston. #2097 (abstract), CD-ROM.

Keller, L.P., McKay, D.S., 1993. Discovery of vapor deposits in the lunar regolith. *Science* **261**, 1305–1307.

Keller, L.P., McKay, D.S., 1997. The nature and origin of rims on lunar soil grains. *Geochim. Cosmochim. Acta* **61** (11), 2331–2341.

Korotev, R.L., Gillis, J.J., 2001. A new look at the Apollo 11 regolith and KREEP. *J. Geophys. Res.* **106** (E6), 12,339–12,354.

Laul, J.C., Vaniman, D.T., Papike, J.J., 1978. Chemistry, mineralogy and petrology of seven >1 mm fragments from Mare Crisium. In: Merrill, R.B., Papike, J.J. (Eds.), *Mare Crisium: The view from Luna 24*. Pergamon Press, New York, pp. 537–568.

Lawrence, D.J., Feldman, W.C., Elphic, R.C., Little, R.C., Prettyman, T.H., Maurice, S., Lucey, P.G., Binder, A.B., 2002. Iron abundances on the lunar surface as measured by the Lunar Prospector gamma-ray and neutron spectrometers. *J. Geophys. Res.* **107** (E12), 5130. doi:10.1029/2001JE001530.

Lee, E.M., 1997. Clementine UV–vis multispectral processing (abstract). *Lunar Planet. Sci.* **XXVIII**, 797–798.

Lucey, P.G., 2004. Mineral maps of the Moon. *Geophys. Res. Lett.* **31**. doi:10.1029/2003GL019406.

Lucey, P.G., Taylor, G.J., Malaret, E., 1995. Abundance and distribution of iron on the Moon. *Science* **268**, 1150–1153.

Lucey, P.G., Blewett, D.T., Hawke, B.R., 1998. Mapping the FeO and TiO_2 content of the lunar surface with multispectral imagery. *J. Geophys. Res.* **103** (E2), 3679–3699.

Lucey, P.G., Blewett, D.T., Jolliff, B.L., 2000a. Lunar iron and titanium abundance algorithms based on final processing Clementine UV–vis images. *J. Geophys. Res.* **105** (E8), 20,297–20,305.

Lucey, P.G., Blewett, D.T., Taylor, G.J., Hawke, B.R., 2000b. Imaging of lunar surface maturity. *J. Geophys. Res.* **105** (E8), 20,377–20,386.

Ma, M.S., Schmitt, R.A., Taylor, G.J., Warner, R.D., Lange, D.E., Keil, K., 1978. Chemistry and petrology of Luna 24 lithic fragments and <250 μm soils: constraints on the origin of VLT mare basalts. In: Merrill, R.B., Papike, J.J. (Eds.), *Mare Crisium: The view from Luna 24*. Pergamon Press, New York, pp. 569–592.

McCord, T.B., Pieters, C.M., Feierberg, M.A., 1976. Multispectral mapping of the lunar surface using ground-based telescopes. *Icarus* **29**, 1–34.

McEwen, A.S., Robinson, M.S., 1997. Mapping of the Moon by Clementine. *Adv. Space Res.* **19** (10), 1523–1533.

McKay, D.S., Heiken, G.H., Basu, A., Blanford, G., Simon, S., Reedy, R.C., French, B.M., Papike, J.J., 1991. The Lunar Regolith. In: Heiken, G.H., Vaniman, D.T. (Eds.), *Lunar Sourcebook: A user's guide to the Moon*. Cambridge Univ. Press, New York, pp. 285–365.

Melendrez, D.E., Johnson, J.R., Larson, S.M., Singer, R.B., 1994. Remote sensing of potential lunar resources, 2. High spatial resolution mapping of spectral reflectance ratios and implications for near side mare TiO_2 content. *J. Geophys. Res.* **99** (E3), 5601–5619.

Morris, R.V., 1978. The surface exposure (maturity) of lunar soils; some concepts and I_s/FeO compilation. In: *Proc. Lunar Planet. Sci. Conf. 9th*, 2287–2297.

Mustard, J.F., Pieters, C.M., 1989. Photometric phase function of common geologic minerals and applications to quantitative analysis of mineral mixture reflectance spectra. *J. Geophys. Res.* **94**, 13,619–13,634.

Noble, S.K., Pieters, C.M., Taylor, L.A., Morris, R.V., Allen, C.C., McKay, D.S., Keller, L.P., 2001. The optical properties of the finest fraction of lunar soil: implications for space weathering. *Meteorit. Planet. Sci.* **36**, 31–42.

Nozette, S. and The Clementine Team, 1994. The Clementine Mission to the Moon: Scientific overview. *Science* **266**, 1835–1839.

Papike, J.J., Vaniman, D.T., 1978. Luna 24 ferrobasalts and the mare basalt suit: comparative chemistry, mineralogy, and petrology. In: Merrill, R.B., Papike, J.J. (Eds.), *Mare Crisium: The View from Luna 24*. Pergamon Press, New York, pp. 371–401.

Papike, J.J., Simon, S.B., Laul, J.C., 1982. The Lunar Regolith: chemistry, mineralogy, petrology. *Rev. Geophys. Space Phys.* **20** (4), 761–826.

Papike, J.J., Taylor, L.A., Simon, S., 1991. Lunar Materials. In: Heiken, G.H., Vaniman, D.T., French, B.M. (Eds.), *Lunar Sourcebook: A User's guide to the Moon*. Cambridge University Press, Cambridge [England]; New York, pp. 121–182.

Papike, J.J., Ryder, G., Shearer, C.K., 1998. Lunar Samples (Ch. 5). In: Ribbe, P.H., Papike, J.J. (Eds.), *Reviews in Mineralogy, Planetary materials*. Mineralogical Society of America, Washington, DC, USA, pp. 5–234.

Pieters, C.M., 1978. Mare basalt types on the front side of the Moon: a summary of spectral reflectance data. In: *Proc. Lunar Planet. Sci. Conf. 9th*, 2825–2849.

Pieters, C.M., 1993. Compositional diversity and stratigraphy of the lunar crust derived from reflectance spectroscopy. In: Englert, P.A.J., Pieters, C.M. (Eds.), *Remote Geochemical Analysis: Elemental and Mineralogical Composition (Topics in Remote Sensing 4)*, xxiii. Cambridge University Press, Cambridge New York, p. 594.

Pieters, C.M., McCord, T.B., 1976. Characterization of lunar mare basalt types: A remote sensing study using reflection spectroscopy of surface soils. In: *Proc. Lunar Sci. Conf. 7th*, 2677–2690.

Pieters, C.M., McCord, T.B., Adams, J.B., 1976. Regional basalt types in the Luna 24 landing area as derived from remote observations. *Geophys. Res. Lett.* **3** (11), 697–700.

Pieters, C.M., Fischer, E.M., Rode, O., Basu, A., 1993. Optical effects of space weathering: the role of the finest fraction. *J. Geophys. Res.* **98** (E11), 20,817–20,824.

Pieters, C.M., Stankevich, D.G., Shkuratov, Y.G., Taylor, L.A., 2002. Statistical analysis of the links among lunar mare soil mineralogy, chemistry, and reflectance spectra. *Icarus* **155** (2), 285–298.

Pieters, C.M., Head, J.W., Adams, J.B., McCord, T.B., Zisk, S.H., Whitford-Stark, J.L., 1980. Late high-titanium basalts of the west maria: geology of the Flamsteed region of Oceanus Procellarum. *J. Geophys. Res.* **85** (B7), 3913–3938.

Pohn, H.A., Wildey, R.L., 1970. A photoelectric–photographic study of the normal albedo of the Moon, accompanied by an Albedo map of the Moon. *USGS Professional Paper 599-E*, E1–E20.

Prettyman, T.H., Hagerty, J., Elphic, R.C., Feldman, W.C., Lawrence, D.J., McKenney, G., Vaniman, D.T., 2006. Elemental composition of the lunar surface: analyses of gammay ray spectroscopy data from Lunar Prospector. *J. Geophys. Res.*, in press.

Rava, B., Hapke, B., 1987. An Analysis of the Mariner 10 color ratio map of Mercury. *Icarus* **71** (3), 397–429.

Rhodes, J.M., 1977. Some compositional aspects of lunar regolith evolution. *Philos. Trans. R. Soc. London* **A285**, 293–301.

Riner, M.A., Robinson, M.S., Tangeman, J.A., Elphic, R.C., 2005. Is ilmenite always the dominant carrier of titanium in lunar mare basalts? *Lunar and Planetary Science XXXVI*, Lunar Planet. Inst., Houston. #1943 (abstract), CD-ROM.

Robinson, M.S., 2001. Scattered Light in the Clementine UV–vis Camera. *Lunar and Planetary Science XXXII*, Lunar Planet. Inst., Houston. #2004 (abstract), CD-ROM.

Schultz, P.H., Spudis, P.D., 1983. Beginning and end of lunar mare volcanism. *Nature* **302**, 233–236.

Simon, S.B., Papike, J.J., Laul, J.C., 1981. The lunar regolith: comparative studies of the Apollo and Luna sites. Petrology of soils from Apollo 17, Luna 16, 20, and 24. *Proc. Lunar Planet. Sci.* **12B**, 371–388.

Staid, M.I., Pieters, C.M., 2001. Mineralogy of the last lunar basalts: results from Clementine. *J. Geophys. Res.* **106** (E11), 27,887–27,900.

Taylor, L.A., 1994. Helium-3 on the Moon: model assumptions and abundances. In: *Engineering, Construction, and Operations in Space IV, Proc. Space '94*, 678–686.

Taylor, L.A., Patchen, A., Taylor, D.S., Chambers, J.G., 1996. X-ray digital imaging petrography of lunar mare soils: modal analyses of minerals and glasses. *Icarus* **124**, 500–512.

Taylor, L.A., Pieters, C., Keller, L.P., Morris, R.V., McKay, D.S., Patchen, A., Wentworth, S., 2001a. The effects of space weathering on Apollo 17 mare soils: petrographic and chemical characterization. *Meteorit. Planet. Sci.*, 285–299.

Taylor, L.A., Pieters, C.M., Keller, L.P., Morris, R.V., McKay, D.S., 2001b. Lunar mare soils: space weathering and the major effects of surface-correlated nanophase Fe. *J. Geophys. Res.* **106** (E11), 27,985–27,999.

Thompson, T.W., 1987. High-resolution lunar radar map at 70-cm wavelength. *Earth Moon Planets* **37**, 59–70.

Walker, R.J., Papike, J.J., 1981. The relationship of the lunar regolith <10 mm fraction and agglutinates. Part II: chemical composition of

agglutinate glass as a test of the "fusion of the finest fraction" (F^3) model. *Proc. Lunar Sci. Conf.* **12B**, 421–432.

Wells, E., Hapke, B., 1977. Lunar soil: iron and titanium bands in the glass fraction. *Science* **195**, 977–979.

Whitaker, E.A., 1972. Lunar color boundaries and their relationship to topographic features. *Moon* **4** (3/4), 348–355.

Wilcox, B.B., Lucey, P.G., Hawke, B.R., 2006. Radiative transfer modeling of compositions of lunar pyroclastic deposits. *J. Geophys. Res.* **111**. doi:10.1029/2006JE002686.

Wilhelms, D.E., 1987. *The geologic history of the Moon* (U.S. Geol. Surv. Prof. Paper 1348). United States Government printing office, Washington, DC.